RSC Advances

PAPER

View Article Online
View Journal | View Issue

Cite this: *RSC Adv.*, 2025, **15**, 30001

Furan–thiazole hydrazone scaffolds as promising antitubercular and antibacterial agents: synthesis, characterization, bioevaluation and computational analysis

Yuvraj R. Sable,[ab] Rahul A. Shinde, *[c] Haya Khader Ahmad Yasin, *[de] Niraj Ghanwate,[f] Suraj N. Mali,[g] Suresh K. Ghotekar,[h] Dhanesh P. Gawari,[b] Dinesh A. Sasane[b] and Vishnu A. Adole *[a]

In the search for novel therapeutic agents against tuberculosis and bacterial infections, a series of furan–thiazole hydrazone derivatives (**4a–4n**) was synthesized, characterized and evaluated for antitubercular and antibacterial properties. The furan–thiazole hydrazone derivatives were characterized using FT-IR, ^{1}H NMR, ^{13}C{^{1}H} NMR, ^{19}F NMR and HRMS methods. The synthesized compounds were tested *in vitro* against *Mycobacterium tuberculosis* H37Rv, *Staphylococcus aureus*, and *Escherichia coli*. Compounds **4a**, **4b** and **4c** exhibited good antitubercular activity with MIC values of 3.12 μg mL^{-1}, comparable to the standard drug pyrazinamide. In antibacterial assays, compound **4g**, bearing a trifluoromethoxy group, demonstrated superior efficacy with inhibition zones of 19 mm (*S. aureus*) and 17 mm (*E. coli*). Molecular docking studies further validated these findings, revealing strong binding affinities of compounds **4a–4c** with *M. tuberculosis* CYP51 (−10.32 to −10.76 kcal mol^{-1}) and compound **4g** with 2,2-dialkylglycine decarboxylase (−9.65 kcal mol^{-1}), suggesting effective interaction with key active site residues. *In silico* ADME profiling revealed favorable drug-likeness and pharmacokinetics for most compounds, while DFT studies including structure optimization, FMO analysis, reactivity descriptors, and MEP mapping offered valuable insights into electronic distribution, reactivity, and potential binding sites of the furan–thiazole hydrazone derivatives. The results support the candidacy of compounds **4a**, **4b** and **4c** in antitubercular study, while **4f** and **4g** as notable antibacterial agents for future development.

Received 15th June 2025
Accepted 18th July 2025

DOI: 10.1039/d5ra04238k

rsc.li/rsc-advances

1 Introduction

Heterocyclic compounds continue to serve as valuable scaffolds in medicinal chemistry, owing to their remarkable structural diversity and broad-spectrum biological activities.[1–3] These compounds, characterized by aromatic or partially saturated ring structures containing at least one heteroatom such as nitrogen, oxygen, and sulfur and are foundational in the design of numerous therapeutic agents. Among them, the thiazole ring system has created interest for its wide-ranging pharmacological applications, including anticancer [4,5] antitubercular [6,7] antimicrobial [8,9] anti-inflammatory [10] antioxidant[11] antidepressant [12] antiviral [13] antidiabetic [14] and antiparasitic[15] properties. Hydrazones, on the other hand, are well-known for their role as effective Schiff base derivatives that exhibit diverse biological properties.[16] When these two moieties are conjugated into thiazole–hydrazone scaffolds, the resulting hybrid system benefits from enhanced conjugation, improved cell permeability, and favourable pharmacodynamic profiles.[17,18] Molecular hybridization, a widely accepted strategy in rational drug design, involves the fusion of two or more bioactive moieties

[a]*Research Centre in Chemistry, Mahatma Gandhi Vidyamandir's Loknete Vyankatrao Hiray Arts, Science and Commerce College, Panchavati, Nashik 422003, Maharashtra, India. E-mail: sabley70@gmail.com; vishnuadole86@gmail.com*

[b]*Department of Chemistry, Dr Patangrao Kadam Mahavidyalaya Ramanandanagar (Burli), Palus 416308, Maharashtra, India. E-mail: dhaneshgawari8@gmail.com; sasanedinesh25@gmail.com*

[c]*Department of Chemistry, Mahatma Gandhi Vidyamandir's Maharaja Sayajirao Gaikwad Arts, Science and Commerce College, Nashik, Malegaon 423105, Maharashtra, India. E-mail: rahulshinde843@gmail.com*

[d]*Department of Pharmaceutical Sciences, College of Pharmacy and Health Sciences, Ajman University, P. O. Box 346, Ajman, United Arab Emirates. E-mail: h.yasin@ajman.ac.ae*

[e]*Center of Medical and Bio-allied Health Sciences Research, Ajman University, P. O. Box 346, Ajman, United Arab Emirates*

[f]*Department of Microbiology, Sant Gadge Baba Amravati University, Amravati 444602, Maharashtra, India. E-mail: nirajghanwate@gmail.com*

[g]*School of Pharmacy, D. Y. Patil University (Deemed to be University), Navi Mumbai 400706, Maharashtra, India. E-mail: mali.suraj1695@gmail.com*

[h]*Centre for Herbal Pharmacology and Environmental Sustainability, Chettinad Hospital and Research Institute, Chettinad Academy of Research and Education, Kelambakkam 603103, Tamil Nadu, India. E-mail: ghotekarsuresh7@gmail.com*

into a single molecular framework to yield compounds with enhanced potency, reduced resistance development, and multifaceted biological activity. The inclusion of the furan ring an oxygen-containing aromatic heterocycle has been associated with a wide range of biological activities, including antimicrobial [19] anticancer [20] antioxidant [21] anti-inflammatory[22] and antimalarial[23] properties. Its planar structure and electron-rich nature enable it to participate effectively in π-stacking and hydrogen bonding interactions, enhancing binding affinity with biological targets.[22,23] In this context, the furan–thiazole hydrazone framework represents a rationally designed hybrid that leverages the therapeutic potential of each constituent pharmacophore. By combining the conjugated features of the hydrazone linkage with the bioactive nature of the thiazole and furan cores, these hybrids can exhibit synergistic or additive effects in targeting microbial enzymes.[24] The versatility of this hybrid approach also allows for structural fine-tuning through strategic substitution, offering opportunities to improve selectivity, pharmacokinetics, and drug-likeness. Nitrofurans and thiazole-containing compounds possess a wide range of pharmacological activities and have been successfully utilized in various therapeutic categories such as antibiotics [25,26] antibacterials [27,28] anti-inflammatory agents [29,30] antineoplastic [31] and nutritional supplements;[32] representative examples of these versatile bioactive molecules are depicted in Fig. 1.

One of the most deadly infectious diseases that contributes significantly to morbidity and death worldwide is tuberculosis (TB), which is caused by the *Mycobacterium tuberculosis* bacteria. Novel chemotherapeutic approaches are urgently needed since the advent of extensively drug-resistant (XDR) and multidrug-resistant (MDR) pathogens has reduced the effectiveness of traditional treatments.[33–36] In this context, heterocyclic compounds, particularly those containing nitrogen and sulfur atoms, have shown remarkable potential as antitubercular agents.[3,7] Likewise, the emergence of antibiotic-resistant bacterial infections poses a serious threat to global health, as increasing resistance in both Gram-positive and Gram-negative bacteria continues to undermine the efficacy of existing treatments.[37–41] Hydrazone-based heterocycles, particularly those incorporating thiazole and furan moieties, have been widely explored for their antimicrobial properties.[42,43] The presence of electron-withdrawing and electron-donating substituents on aryl rings significantly influences antibacterial potency by modulating lipophilicity, electronic distribution, and membrane permeability.[9,43] Thus, the design of new furan–thiazole hydrazone derivatives with diverse substitution patterns offer a strategic approach to synthesize agents effective against various bacterial strains.

In addition to experimental bioevaluation, computational chemistry has emerged as an essential tool in modern drug discovery.[44] Density Functional Theory (DFT) calculations enable detailed analysis of molecular geometry, frontier molecular orbitals (HOMO–LUMO), and global reactivity descriptors, providing insight into the electronic structure and

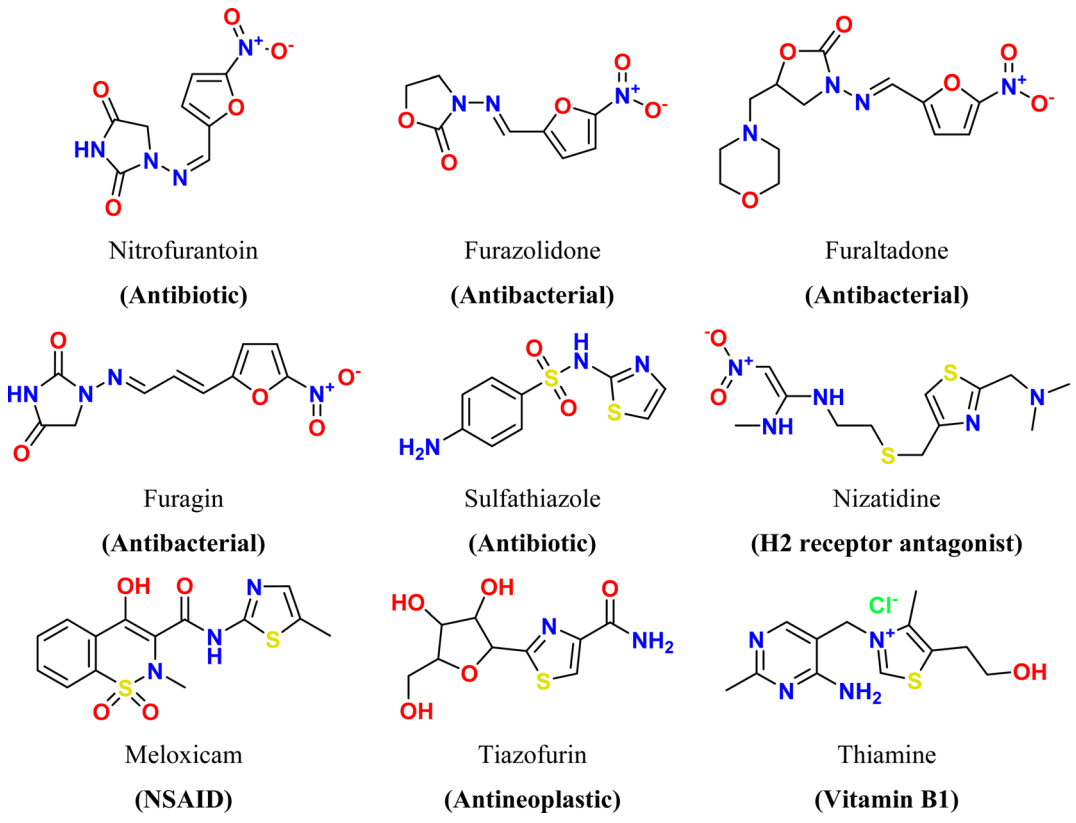

Fig. 1 Representative examples of biologically active compounds containing nitrofuran and thiazole scaffolds with diverse therapeutic applications.

chemical reactivity of molecules. Molecular Electrostatic Potential (MEP) maps further assist in visualizing charge distribution, which is critical for predicting reactive sites.[45–48] Moreover, molecular docking studies allow the prediction of binding modes and affinities of small molecules with biological targets.[49–51] To complement these analyses, ADME (Absorption, Distribution, Metabolism, and Excretion) profiling is performed to assess pharmacokinetic properties and drug-likeness.[52–54] In this study, a series of furan–thiazole hydrazone derivatives were synthesized and characterized, followed by evaluation of their antitubercular and antibacterial activities. A combined experimental and computational approach was employed to explore their structure–activity relationships, electronic features, and pharmacokinetic potential, aiming to identify promising leads for future antitubercular and antibacterial drug development.

2 Materials and methods

2.1. General remarks

All chemicals and reagents used in the present study were of analytical grade. The progress of reactions was monitored by thin-layer chromatography (TLC) using pre-coated silica gel 60 F_{254} plates (Merck) and visualized under UV light (254/365 nm). Melting points were determined using an open capillary method and are uncorrected. Fourier-transform infrared (FT-IR) spectra were recorded on a Bruker FT-IR spectrophotometer. Proton (^{1}H), carbon (^{13}C{^{1}H}) and fluorine (^{19}F) NMR spectra were obtained on a Bruker Avance III 500 MHz spectrometer using DMSO-d_6 as the solvent and tetramethylsilane (TMS) as the internal standard. The high resolution mass spectrometry (HRMS) using ESI mode was used to record the HRMS of all synthesized compounds. Chemical shifts (δ) are reported in parts per million (ppm), and coupling constants (J) are expressed in Hertz (Hz). The purity of the synthesized compounds was confirmed by TLC and spectral consistency.

2.2. Synthesis of (*E*)-2-(2-((5-nitrofuran-2-yl)methylene) hydrazinyl)-4-arylthiazole derivatives (4a–4n)

The furan–thiazole hydrazone derivatives (**4a–4n**) were synthesized *via* a one-pot, three-component condensation reaction, as detailed below (Scheme 1). A mixture of 5-nitrofuran-2-carbaldehyde (**1**, 2 mmol) and thiosemicarbazide (**2**, 2 mmol) were refluxed for one hour and after this the selected phenacyl bromide derivatives (**3a–3n**, 2 mmol) were added in ethanol (10 mL). Progress of the reaction was monitored by thin-layer chromatography (TLC) using a hexane/ethyl acetate (8 : 2) solvent system. After completion of the reaction, the mixture was cooled to room temperature (reaction time: nearly 1.5 hours). The resulting solid product was filtered, washed with cold ethanol, and dried. The crude products were then recrystallized from ethanol to afford pure compounds **4a–4n**.

2.3. Spectral data (*E*)-2-(2-((5-nitrofuran-2-yl)methylene) hydrazinyl)-4-arylthiazole derivatives (4a–4n)

2.3.1. (*E*)-2-(2-((5-Nitrofuran-2-yl)methylene)hydrazinyl)-4-(4-nitrophenyl)thiazole (4a). Maroon colour; yield: 95%; m.p. 220–222 °C; FT-IR (cm^{-1}): 3257, 3084, 1569, 1482, 1416, 1330, 1243, 1193, 1148, 1107, 1053, 1016, 966, 900, 855, 789, 727, 578; ^{1}H NMR (500 MHz, DMSO-d_6) δ 12.85 (s, 1H), 8.29 (d, J = 8.9 Hz, 2H), 8.12 (d, J = 8.9 Hz, 2H), 7.99 (s, 1H), 7.83 (s, 1H), 7.78 (d, J = 3.9 Hz, 1H), 7.16 (d, J = 3.9 Hz, 1H); ^{13}C{^{1}H} NMR (126 MHz, DMSO-d_6) δ 168.1, 152.3, 152.1, 149.2, 146.8, 140.8, 129.9, 126.9, 124.7, 115.6, 114.6, 110.2; HRMS (ESI) for $C_{14}H_9N_5O_5S$: calculated $(M + H)^+$: 360.0402 and observed $(M + H)^+$: 360.0404.

2.3.2. (*E*)-4-(4-Chlorophenyl)-2-(2-((5-nitrofuran-2-yl) methylene)hydrazinyl)thiazole (4b). Maroon colour; yield: 94%; m.p. 214–216 °C; FT-IR (cm^{-1}): 3624, 3117, 2943, 1619, 1577, 1462, 1396, 1330, 1243, 1193, 1140, 1090, 1020, 958, 909, 801, 731; ^{1}H NMR (500 MHz, DMSO-d_6) δ 12.76 (s, 1H), 7.98 (s, 1H), 7.88 (d, J = 8.6 Hz, 2H), 7.78 (d, J = 3.9 Hz, 1H), 7.50 (s, 1H), 7.48 (d, J = 8.6 Hz, 2H), 7.14 (d, J = 3.9 Hz, 1H); ^{13}C{^{1}H} NMR (126

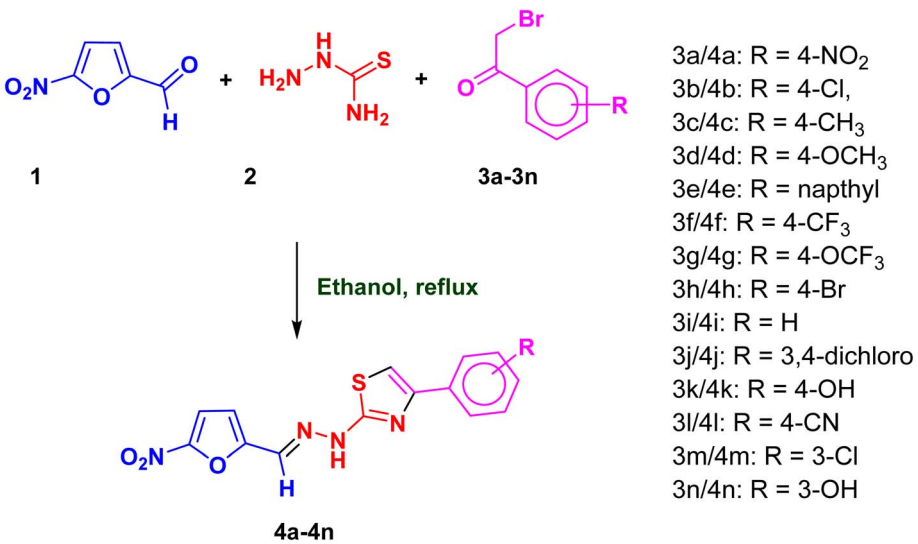

Scheme 1 Synthesis of furan–thiazole hydrazone derivatives.

MHz, DMSO-d_6) δ 167.8, 152.5, 152.1, 149.8, 133.7, 132.6, 129.6, 129.2, 127.7, 115.6, 114.3, 106.2; HRMS (ESI) for $C_{14}H_9ClN_4O_3S$: calculated $(M + H)^+$: 349.0162 and observed $(M + H)^+$: 349.0156 and $(M + H + 2)^+$: 351.0126.

2.3.3. (*E*)-2-(2-((5-Nitrofuran-2-yl)methylene)hydrazinyl)-4-(*p*-tolyl)thiazole (4c). Red orange colour; yield: 88%; m.p. 180–182 °C; FT-IR (cm^{-1}): 3637, 3117, 2923, 2857, 1614, 1577, 1503, 1474, 1325, 1247, 1193, 1107, 1024, 971, 904, 810, 744, 657, 587; ^1H NMR (500 MHz, DMSO-d_6) δ 12.69 (s, 1H), 7.98 (s, 1H), 7.78 (d, $J = 3.9$ Hz, 1H), 7.75 (d, $J = 8.1$ Hz, 2H), 7.36 (s, 1H), 7.22 (d, $J = 8.1$ Hz, 2H), 7.14 (d, $J = 3.9$ Hz, 1H), 2.32 (s, 3H); $^{13}C\{^1H\}$ NMR (126 MHz, DMSO-d_6) δ 167.6, 152.6, 152.0, 150.9, 137.5, 132.1, 129.7, 129.4, 126.0, 115.6, 114.2, 104.4, 21.3; HRMS (ESI) for $C_{15}H_{12}N_4O_3S$: calculated $(M + H)^+$: 329.0708 and observed $(M + H)^+$: 329.0705.

2.3.4. (*E*)-4-(4-Methoxyphenyl)-2-(2-((5-nitrofuran-2-yl) methylene)hydrazinyl)thiazole (4d). Brown colour; yield: 87%; m.p. 202–204 °C; FT-IR (cm^{-1}): 3620, 3137, 3075, 2972, 2877, 1631, 1573, 1474, 1334, 1239, 1144, 1024, 958, 909, 805, 727, 673, 578; ^1H NMR (500 MHz, DMSO-d_6) δ 12.73 (s, 1H), 7.97 (s, 1H), 7.83–7.76 (m, 3H), 7.26 (s, 1H), 7.13 (d, $J = 3.9$ Hz, 1H), 6.98 (d, $J = 8.8$ Hz, 2H), 3.79 (s, 3H); $^{13}C\{^1H\}$ NMR (126 MHz, DMSO-d_6) δ 167.6, 159.4, 152.6, 152.0, 129.8, 129.3, 127.6, 127.4, 115.6, 114.5, 114.2, 103.2, 55.6; HRMS (ESI) for $C_{15}H_{12}N_4O_4S$: calculated $(M + H)^+$: 345.0657 and observed $(M + H)^+$: 345.0654.

2.3.5. (*E*)-4-(Naphthalen-2-yl)-2-(2-((5-nitrofuran-2-yl) methylene)hydrazinyl)thiazole (4e). Red orange colour; yield: 85%; m.p. 189–191 °C; FT-IR (cm^{-1}): 3364, 3175, 3129, 1610, 1565, 1519, 1478, 1317, 1243, 1193, 1008, 909, 855, 810, 748, 669, 574; ^1H NMR (500 MHz, DMSO-d_6) δ 12.86 (s, 1H), 8.39 (s, 1H), 8.05–7.89 (m, 5H), 7.79 (d, $J = 3.9$ Hz, 1H), 7.60 (s, 1H), 7.57–7.45 (m, 2H), 7.16 (d, $J = 3.9$ Hz, 1H); $^{13}C\{^1H\}$ NMR (126 MHz, DMSO-d_6) δ 167.8, 152.6, 152.0, 150.9, 133.6, 133.0, 132.2, 129.5, 128.7, 128.3, 128.1, 127.0, 126.6, 124.7, 124.3, 115.6, 114.3, 106.2; HRMS (ESI) for $C_{18}H_{12}N_4O_3S$: calculated $(M + H)^+$: 365.0708 and observed $(M + H)^+$: 365.0703.

2.3.6. (*E*)-2-(2-((5-Nitrofuran-2-yl)methylene)hydrazinyl)-4-(4-(trifluoromethyl)phenyl)thiazole (4f). Red orange colour; yield: 82%; m.p. 197–199 °C; FT-IR (cm^{-1}): 3216, 3113, 2985, 2865, 2725, 1569, 1478, 1338, 1243, 1185, 1127, 1024, 958, 904, 801, 739, 698, 574; ^1H NMR (500 MHz, DMSO-d_6) δ 12.82 (s, 1H), 8.07 (d, $J = 8.1$ Hz, 2H), 7.99 (s, 1H), 7.82–7.77 (m, 3H), 7.68 (s, 1H), 7.15 (d, $J = 3.9$ Hz, 1H); $^{13}C\{^1H\}$ NMR (126 MHz, DMSO-d_6) δ 167.9, 153.1, 152.4, 152.1, 149.7, 138.6, 130.3, 129.7, 126.6, 126.2, 126.1, 125.9, 123.7, 115.6, 115.6, 114.5, 113.7, 108.2; ^{19}F NMR (471 MHz, DMSO-d_6) δ −60.90; HRMS (ESI) for $C_{15}H_9F_3N_4O_3S$: calculated $(M + H)^+$: 383.0425 and observed $(M + H)^+$: 383.0425.

2.3.7. (*E*)-2-(2-((5-Nitrofuran-2-yl)methylene)hydrazinyl)-4-(4-(trifluoromethoxy)phenyl)thiazole (4g). Red orange colour; yield: 80%; m.p. 180–182 °C; FT-IR (cm^{-1}): 3414, 3137, 1594, 1482, 1338, 1206, 1107, 1024, 962, 921, 818, 739, 578; ^1H NMR (500 MHz, DMSO-d_6) δ 12.79 (s, 1H), 8.00–7.96 (m, 3H), 7.78 (d, $J = 3.9$ Hz, 1H), 7.53 (s, 1H), 7.42 (d, $J = 8.4$ Hz, 2H), 7.15 (d, $J = 3.9$ Hz, 1H); $^{13}C\{^1H\}$ NMR (126 MHz, DMSO-d_6) δ 169.0, 148.9, 148.5, 148.0, 148.0, 147.6, 139.4, 136.8, 134.2, 129.3, 127.8, 124.8, 121.7, 119.6, 109.0, 104.8, 66.8, 50.8, 15.3; ^{19}F NMR (471 MHz, DMSO-d_6) δ −56.75; HRMS (ESI) for $C_{15}H_9F_3N_4O_4S$: calculated $(M + H)^+$: 399.0374 and observed $(M + H)^+$: 399.0376.

2.3.8. (*E*)-4-(4-Bromophenyl)-2-(2-((5-nitrofuran-2-yl) methylene)hydrazinyl)thiazole (4h). Maroon colour; yield: 84%; m.p. 199–201 °C; FT-IR (cm^{-1}): 3629, 3084, 2960, 2865, 1627, 1577, 1470, 1334, 1235, 1140, 1061, 1012, 962, 904, 797, 731, 686, 550; ^1H NMR (500 MHz, DMSO-d_6) δ 12.76 (s, 1H), 7.98 (s, 1H), 7.81 (d, $J = 8.5$ Hz, 2H), 7.78 (d, $J = 3.9$ Hz, 1H), 7.61 (d, $J = 8.6$ Hz, 2H), 7.52 (s, 1H), 7.14 (d, $J = 3.9$ Hz, 1H); $^{13}C\{^1H\}$ NMR (126 MHz, DMSO-d_6) δ 167.8, 152.5, 152.1, 134.0, 132.1, 129.6, 128.0, 121.2, 119.7, 115.6, 114.4, 106.3; HRMS (ESI) for $C_{14}H_9BrN_4O_3S$: calculated $(M + H)^+$: 392.9656 and observed $(M + H)^+$: 392.9657 and $(M + H + 2)^+$: 394.9631.

2.3.9. (*E*)-2-(2-((5-Nitrofuran-2-yl)methylene)hydrazinyl)-4-phenylthiazole (4i). Red orange colour; yield: 86%; m.p. 218–220 °C; FT-IR (cm^{-1}): 3166, 3071, 2935, 1552, 1470, 1433, 1325, 1239, 1193, 1136, 1057, 1008, 900, 805, 719, 686, 570; ^1H NMR (500 MHz, DMSO-d_6) δ 12.76 (s, 1H), 7.98 (s, 1H), 7.89–7.84 (m, $J = 7.4$ Hz, 2H), 7.78 (d, $J = 3.9$ Hz, 1H), 7.47–7.39 (m, 3H), 7.32 (t, $J = 7.3$ Hz, 1H), 7.14 (d, $J = 3.9$ Hz, 1H); $^{13}C\{^1H\}$ NMR (126 MHz, DMSO-d_6) δ 167.6, 152.6, 152.0, 134.9, 129.4, 129.3, 129.2, 128.2, 126.0, 115.6, 114.3, 105.4; HRMS (ESI) for $C_{14}H_{10}N_4O_3S$: calculated $(M + H)^+$: 315.0551 and observed $(M + H)^+$: 315.0548.

2.3.10. (*E*)-4-(3,4-Dichlorophenyl)-2-(2-((5-nitrofuran-2-yl) methylene)hydrazinyl)thiazole (4j). Red orange colour; yield: 90%; m.p. 170–172 °C; FT-IR (cm^{-1}): 3125, 1619, 1474, 1321, 1247, 1202, 1148, 1065, 1020, 933, 871, 810, 739, 673, 587; ^1H NMR (500 MHz, DMSO-d_6) δ 12.78 (s, 1H), 8.09 (d, $J = 2.0$ Hz, 1H), 7.98 (s, 1H), 7.85 (dd, $J = 8.4$, 2.0 Hz, 1H), 7.78 (d, $J = 3.9$ Hz, 1H), 7.68 (d, $J = 8.4$ Hz, 1H), 7.66 (s, 1H), 7.15 (d, $J = 3.9$ Hz, 1H); $^{13}C\{^1H\}$ NMR (126 MHz, DMSO-d_6) δ 167.9, 152.4, 152.1, 148.5, 135.4, 132.0, 131.4, 130.4, 129.7, 127.7, 126.1, 115.6, 114.5, 107.6; HRMS (ESI) for $C_{14}H_8Cl_2N_4O_3S$: calculated $(M + H)^+$: 382.9772 and observed $(M + H)^+$: 382.9766, $(M + H + 2)^+$: 384.9737 and $(M + H + 2)^+$: 386.9712.

2.3.11. (*E*)-4-(2-(2-((5-Nitrofuran-2-yl)methylene) hydrazinyl)thiazol-4-yl)phenol (4k). Red orange colour; yield: 82%; m.p. 209–211 °C; FT-IR (cm^{-1}): 3459, 3302, 3084, 2968, 1589, 1540, 1453, 1392, 1350, 1251, 1189, 1107, 1024, 958, 904, 830, 731, 649, 562; ^1H NMR (500 MHz, DMSO-d_6) δ 12.86 (s, 1H), 7.97 (s, 1H), 7.78 (d, $J = 3.9$ Hz, 1H), 7.67 (d, $J = 8.6$ Hz, 2H), 7.15 (s, 1H), 7.13 (d, $J = 3.9$ Hz, 1H), 6.79 (d, $J = 8.6$ Hz, 2H); $^{13}C\{^1H\}$ NMR (126 MHz, DMSO-d_6) δ 167.5, 157.7, 152.7, 152.0, 129.8, 129.3, 127.4, 126.1, 115.8, 115.7, 114.2, 102.3; HRMS (ESI) for $C_{14}H_{10}N_4O_4S$: calculated $(M + H)^+$: 331.0501 and observed $(M + H)^+$: 331.0495.

2.3.12. (*E*)-4-(2-(2-((5-Nitrofuran-2-yl)methylene) hydrazinyl)thiazol-4-yl)benzonitrile (4l). Red orange colour; yield: 84%; m.p. 232–233 °C; FT-IR (cm^{-1}): 3249, 3129, 2997, 2217, 1573, 1478, 1404, 1346, 1317, 1239, 1173, 1057, 1020, 962, 904, 834, 706, 562; ^1H NMR (500 MHz, DMSO-d_6) δ 12.81 (s, 1H), 8.04 (d, $J = 8.3$ Hz, 2H), 7.99 (s, 1H), 7.88 (d, $J = 8.3$ Hz, 2H), 7.78 (d, $J = 3.9$ Hz, 1H), 7.74 (s, 1H), 7.15 (d, $J = 3.9$ Hz, 1H); $^{13}C\{^1H\}$ NMR (126 MHz, DMSO-d_6) δ 168.0, 152.4, 152.1, 149.5, 138.9, 133.2, 129.8, 126.6, 119.4, 115.6, 114.5, 110.3, 109.2; HRMS (ESI) for $C_{15}H_9N_5O_3S$: calculated $(M + H)^+$: 340.0504 and observed $(M + H)^+$: 340.0463.

2.3.13. (*E*)-4-(3-Chlorophenyl)-2-(2-((5-nitrofuran-2-yl) methylene)hydrazinyl)thiazole (4m). Brown colour; yield: 83%; m.p. 152–154 °C; FT-IR (cm^{-1}): 3624, 3080, 2972, 1639, 1573, 1474, 1434, 1235, 1148, 1024, 953, 810, 719, 541; ^{1}H NMR (500 MHz, DMSO-d_6) δ 12.78 (s, 1H), 7.98 (s, 1H), 7.91 (t, J = 1.7 Hz, 1H), 7.83 (d, J = 7.8 Hz, 1H), 7.78 (d, J = 3.9 Hz, 1H), 7.60 (s, 1H), 7.45 (t, J = 7.9 Hz, 1H), 7.37 (dd, J = 7.9, 1.1 Hz, 1H), 7.15 (d, J = 3.9 Hz, 1H); ^{13}C{^{1}H} NMR (126 MHz, DMSO-d_6) δ 167.8, 152.5, 152.1, 149.5, 136.8, 134.0, 131.1, 129.6, 127.9, 125.7, 124.5, 115.6, 114.4, 107.0; HRMS (ESI) for $C_{14}H_9ClN_4O_3S$: calculated $(M + H)^+$: 349.0162 and observed $(M + H)^+$: 349.0153.

2.3.14. (*E*)-3-(2-(2-((5-Nitrofuran-2-yl)methylene) hydrazinyl)thiazol-4-yl)phenol (4n). Maroon colour; yield: 83%; m.p. 210–212 °C; FT-IR (cm^{-1}): 3612, 3467, 3088, 2964, 2865, 1577, 1482, 1404, 1325, 1243, 1156, 1111, 1065, 1020, 958, 896, 843, 810, 731, 690, 562; ^{1}H NMR (500 MHz, DMSO-d_6) δ 12.79 (s, 1H), 10.84 (s, 1H), 7.99 (s, 1H), 7.86 (dd, J = 7.8, 1.2 Hz, 1H), 7.78 (d, J = 3.9 Hz, 1H), 7.52 (s, 1H), 7.18–7.14 (m, 2H), 6.93–6.90 (m, 1H), 6.88–6.85 (m, 1H); ^{13}C{^{1}H} NMR (126 MHz, DMSO-d_6) δ 166.8, 155.5, 152.4, 152.1, 148.4, 138.6, 129.9, 129.4, 128.0, 119.6, 117.1, 115.6, 114.5, 106.5; HRMS (ESI) for $C_{14}H_{10}N_4O_4S$: calculated $(M + H)^+$: 331.0501 and observed $(M + H)^+$: 331.0493.

2.4. Anti-tubercular screening method

The furan–thiazole hydrazone derivatives (**4a–4n**) were assessed for antitubercular activity against *Mycobacterium tuberculosis* H37Rv (ATCC 27294) using the Microplate Alamar Blue Assay (MABA) [55] a widely accepted method due to its non-toxic nature, reagent stability, and strong agreement with proportional and BACTEC radiometric assays. The compounds were tested across a concentration range of 100 to 0.8 μg mL^{-1}. To prepare the 96-well plates, 200 μL of sterile deionized water was added to the outer wells to minimize evaporation, while 100 μL of Middlebrook 7H9 broth was added to each test well, followed by serial dilutions of the compounds. Plates were sealed with parafilm and incubated at 37 °C for five days. Subsequently, 25 μL of a freshly prepared 1 : 1 mixture of alamar blue reagent and 10% Tween 80 were added to each well and incubated for another 24 hours. Wells retaining a blue color indicated no bacterial growth, whereas a pink color denoted growth. The minimum inhibitory concentration (MIC) was defined as the lowest concentration preventing this color change. Standard drugs-isoniazid, ethambutol, pyrazinamide, rifampicin, and streptomycin served as positive controls.

2.5. Kirby–Bauer disk diffusion method

The antimicrobial susceptibility testing of the synthesized furan–thiazole hydrazone derivatives (**4a–4n**) was evaluated against *Staphylococcus aureus* (ATCC 23235) and *Escherichia coli* (ATCC 25922) using the standard Kirby–Bauer disk diffusion method.[56] Mueller–Hinton agar plates were prepared and uniformly inoculated with bacterial suspensions adjusted to the 0.5 McFarland standard (approximately 1.5 × 10^8 CFU mL^{-1}). Sterile filter paper discs (6 mm diameter) were impregnated with 30 μL of compound solutions (1 mg mL^{-1} in DMSO) and air-dried under aseptic conditions. These discs were carefully placed on the surface of the inoculated agar plates along with standard antibiotic discs (tetracycline) as positive controls and DMSO-loaded discs as negative controls. All plates were incubated at 37 °C for 24 hours under standard conditions. After incubation, the diameter of the zone of inhibition around each disc was measured in millimeters (mm) using a transparent ruler. The results were interpreted based on inhibition zones, where larger zones indicated stronger antibacterial activity.

2.6. Microbroth dilution method

The Minimum Inhibitory Concentration (MIC) of the synthesized compounds (only those compounds that showed a zone of inhibition) against *Staphylococcus aureus* (ATCC 23235) and *Escherichia coli* (ATCC 25922) was determined using the microbroth dilution method as per CLSI guidelines.[57] Stock solutions of each compound were prepared at a concentration of 1024 μg mL^{-1} using DMSO or sterile distilled water as a solvent. Two-fold serial dilutions were performed in Cation Adjusted Mueller–Hinton Broth (CA-MHB) to obtain a range of concentrations typically from 1024 to 1 μg mL^{-1}. Each dilution (100 μL) was dispensed into the wells of a sterile 96-well microtiter plate. Bacterial inocula were prepared by suspending freshly grown colonies (18–24 hours old) in sterile saline and adjusting the turbidity to match the 0.5 McFarland standard (approximately 1.5 × 10^8 CFU mL^{-1}). The suspension was then diluted 1 : 100 in CA-MHB to achieve a final concentration of approximately 1–2 × 10^6 CFU mL^{-1}. To each well containing the compound dilutions, 100 μL of the bacterial suspension was added, resulting in a final volume of 200 μL per well and a final inoculum density of ~5 × 10^5 CFU mL^{-1}. The plates were incubated at 37 °C for 18–24 hours under aerobic conditions. After incubation, wells were examined visually for turbidity as well as colorimetrically. Each assay included a sterility control (media and compound only), a growth control (bacteria with no compound), and a positive control (standard antibiotic).

2.7. Molecular docking studies

In this study, we employed molecular docking simulations to investigate the binding interactions of a series of furan–thiazole hydrazones (**4a–4n**) with antitubercular target: *Mycobacterium tuberculosis* Cytochrome P450 14α-sterol demethylase (CYP51; PDB ID: 1E9X; resolution: 2.10 Å; **https://www.rcsb.org/structure/1E9X**),[58] and antibacterial target: 2,2-dialkylglycine decarboxylase (PDB ID: 1D7U; resolution: 1.95 Å; **https://www.rcsb.org/structure/1D7U**), both of which have been previously reported in the literature as relevant targets.[59–63] Docking calculations were conducted using 'AutoDockTools' version 1.5.6.[64] A grid box with dimensions 20 × 20 × 20 Å (volume: 8000 $Å^3$)[65] was centered on the co-crystallized ligand 'PIM' in the CYP51 active site and used for further simulations. For processing of protein, we followed all steps such as removal of water molecules, additions of missing side chains, additions of missing residues and Gasteiger charges, and nonpolar hydrogens were applied. As per the 'AutoDock4' (AD4) user manual, we maintained the LGA (the Lamarckian Genetic Algorithm) algorithm and the scoring function

parameters.[64,65] For ligand preparations, we used 'ChemSketch V. 2025' for drawing 2D and then subsequently, 3D structures. Before saving all structures in '.pdbqt', we optimized them with B3LYP/6-31G(d,p) as the basis set. With an exhaustiveness set to 32, docking results were retrieved and visualization for 'ligand–receptor interactions' were done using 'PyMol' (for academic use; **https://pymol.org/edu/**) and 'Discovery Studio Visualizer' V. 2025 (**https://discover.3ds.com/discovery-studio-visualizer-download**). (Note: The apparent shift in double bond positions in the ligand structure is a visualization artefact caused by the loss of bond order information during conversion to PDBQT format for AutoDock. The original chemical structure remains unchanged.)

2.8. Theoretical predictions for ADME

Furan–thiazole-containing compounds were evaluated for their ADME properties using the SwissADME web tool [66] which provides insights into absorption, distribution, metabolism, and excretion profiles based on structure, helping assess drug-likeness and pharmacokinetic behavior. To evaluate the drug-likeness and ADME (Absorption, Distribution, Metabolism, and Excretion) profiles of a series of furan–thiazole hydrazones (**4a–4n**), we utilized the widely used web server SwissADME (**http://www.swissadme.ch/citing.php**; accessed on 10 June 2025).

2.9. DFT method

DFT has emerged as a powerful computational approach for investigating the electronic structure, chemical stability, and reactivity profiles of a wide range of small organic molecules. This method provides valuable theoretical insights that support experimental findings and aid in the rational design of compounds for chemical and pharmacological applications.[67–69] In the present study, all DFT-based quantum chemical calculations for the newly synthesized derivatives (**4a–4n**) were performed in the gas phase utilizing the Gaussian 03 computational package.[70] The electronic properties were evaluated using the B3LYP functional, which combines Becke's three-parameter exchange functional with the Lee–Yang–Parr correlation functional [71,72] in conjunction with the 6-31G(d,p) basis set. Visualization and interpretation of the optimized molecular geometries and frontier molecular orbitals were facilitated using the GaussView version 4.1.2 graphical interface.[73]

3 Results and discussion

3.1. Chemistry and spectral characterization

The target compounds **4a–4n** were synthesized *via* a one-pot, three-component condensation reaction involving 5-nitrofuran-2-carbaldehyde (**1**), thiosemicarbazide (**2**), and different phenacyl bromides (**3a–3n**) in ethanol under reflux conditions.[74] The presence of an electron-deficient aldehyde moiety and the nucleophilic nature of thiosemicarbazide facilitated the initial condensation to form the corresponding thiosemicarbazone intermediate. Subsequently, *in situ* reaction with phenacyl bromide derivatives afforded the final (*E*)-2-(2-((5-nitrofuran-2-yl)methylene)hydrazinyl)-4-arylthiazole derivatives (**4a–4n**) in good yields. The progress of the reaction was monitored by TLC using a hexane/ethyl acetate (8 : 2) solvent system. Upon completion (typically within 2 hours), the precipitated products were collected by filtration, washed with cold ethanol to remove impurities, and recrystallized from ethanol to yield analytically pure compounds. The structures of the synthesized compounds were confirmed by FT-IR, ^{1}H NMR, ^{13}C{^{1}H} NMR and HRMS analyses, which were consistent with the proposed thiazole molecular frameworks.[74] The hydrazone derivatives are proposed to exist predominantly in the *E* configuration across the C=N bond, as this is the more thermodynamically stable form due to minimized steric repulsion between the adjacent substituents. This assignment is consistent with previously reported structural trends for similar hydrazone frameworks in the literature.[75,76] The structural diversity of the synthesized compounds is illustrated in Fig. 2, which showcases a wide range of functional groups incorporated into the molecular framework. These include both electron-donating groups, as well as electron-withdrawing groups. The inclusion of such substituents on the aromatic ring significantly influences the physicochemical properties, electronic distribution, and potentially the biological activity of the resulting furan–thiazole hydrazone derivatives. This diversity allows for systematic structure–activity relationship (SAR) studies and highlights the synthetic versatility.

The FT-IR spectral analysis of the synthesized compounds **4a–4n** confirms the presence of key functional groups consistent with their proposed structures. Broad absorption bands around 3600–3200 cm^{-1} in correspond to N–H or O–H stretching vibrations, indicating the presence of hydrazone[74] or hydroxyl functionalities. Aromatic and aliphatic C–H stretching vibrations are observed in the range of 3100–2850 cm^{-1} across all compounds.[74] Strong bands around 1600–1500 cm^{-1}, are attributed to C=N and aromatic C=C stretching.[74] The presence of nitro groups is supported by asymmetric and symmetric NO_2 stretching vibrations observed in the range of 1540–1320 cm^{-1}. A sharp absorption near 2217 cm^{-1} in **4l** confirms the presence of a nitrile (C≡N) group. The C–O stretching band for phenolic groups appears around 1250–1200 cm^{-1}, notably in **4d**, **4k**, and **4n**. Thiazole and aromatic ring deformations are evident from multiple bands between 1140–540 cm^{-1} across the series. These IR spectra provide crucial insights into the structural motifs of the compounds and support successful synthesis. The ^{1}H NMR spectra of compounds **4a–4n** exhibit characteristic signals confirming the proposed structures. All compounds display a singlet around δ 12.7–12.9, corresponding to the NH proton of the hydrazone moiety. For **4a**, aromatic protons from the nitrophenyl ring appear as doublets at δ 8.29 and 8.12 (J = 8.9 Hz, 2H each), while the furan protons resonate as singlets and doublets between δ 7.16–7.99. In **4b**, the 4-chlorophenyl protons show symmetrical doublets at δ 7.88 and 7.48 (J = 8.6 Hz), and furan resonances appear between δ 7.14–7.98. **4c** contains a *p*-tolyl group, reflected in the methyl singlet at δ 2.32 and aromatic doublets at δ 7.22 and 7.75. In **4d**, the

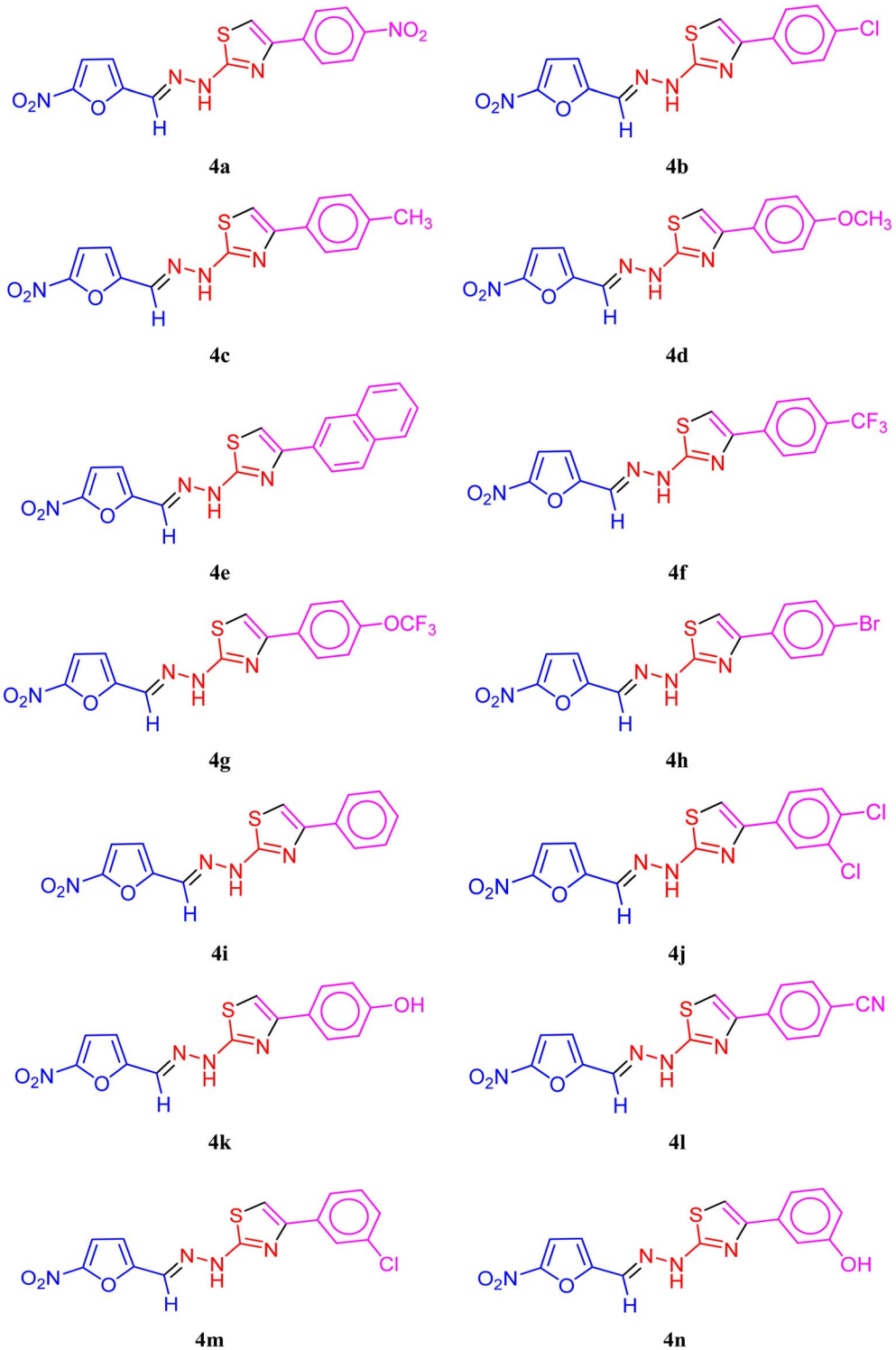

Fig. 2 Structural diversity of synthesized furan–thiazole hydrazone derivatives (**4a–4n**) bearing diverse substitution on the aromatic ring.

presence of a methoxy group is evident by a singlet at δ 3.79, while aromatic protons are observed between δ 6.98–7.83. The **4e** compound with a naphthyl ring shows complex multiplets between δ 7.45–8.39 due to the multiple aromatic protons. **4f** and **4g**, having trifluoromethyl and trifluoromethoxy groups, display chemical shifts of aromatic protons, with multiplets and singlets appearing around δ 7.42–8.07. **4h**, bearing a bromophenyl group, shows well-defined aromatic doublets at δ 7.81 and 7.61. In **4i**, the phenyl protons appear as a multiplet from δ 7.32–7.89. **4j** shows distinctive aromatic signals due to the 3,4-dichlorophenyl ring, including a doublet of doublets at δ 7.85. **4k** contains a phenolic ring, evident by doublets at δ 6.79 and

7.67. In **4l**, the benzonitrile moiety shows typical doublets at δ 8.04 and 7.88. **4m**, with a 3-chlorophenyl ring, shows aromatic protons distributed between δ 7.37–7.91. Lastly, **4n**, containing a phenol ring at the *meta*-position, exhibits an additional OH signal at δ 10.84 and aromatic multiplets between δ 6.85–7.86 ppm. The $^{13}C\{^1H\}$ NMR spectra of compounds **4a–4n** are consistent with their structures, typically showing 12–18 carbon signals. The carbon of the imine (C=N) or hydrazone linkage is observed downfield around δ 167–169 in all compounds. Nitro and furan-related quaternary carbons appear around δ 150–153. In **4a**, resonances at δ 168.10, 152.33, and 149.16 support the presence of a thiazole ring. Similar types of signals were observed for rest of the compounds. The compound **4b** shows chlorophenyl carbons between δ 127.72–133.67. In **4c**, the methyl carbon of the *p*-tolyl group appears at δ 21.28, and aromatic carbons between δ 104.44–137.53. **4d** displays the methoxy carbon at δ 55.61 and aromatic carbons consistent with substituted anisole. The naphthyl carbons in **4e** give multiple signals from δ 124.34 to 133.59. In **4f** and **4g**, the presence of fluorinated substituents results in deshielded carbon signals above δ 148. **4h** shows aromatic bromophenyl carbons from δ 128.04–134.03. In **4i**, the phenyl ring gives signals around δ 128–129. **4j**, with two chlorine substituents, gives additional downfield peaks near δ 148.53 and 135.36. **4k** and **4n**, which include phenol functionalities, exhibit resonances near δ 157–158 for the phenolic carbon. The cyano carbon in **4l** is evident around δ 110.26. Lastly, **4m** shows aromatic carbon resonances at δ 124.54–136.82 due to the 3-chlorophenyl ring. The ^1H and $^{13}C\{^1H\}$ NMR data collectively confirm the proposed structures of all 14 thiazole-hydrazone derivatives. The *para*-substituted trifluoromethyl derivative **4f** exhibits a single, strong singlet at δ −60.90 in the ^{19}F NMR spectra, which is indicative of an aryl-CF_3 group. The analogous resonance is shifted downfield to δ −56.75 when an intervening oxygen atom is added to compound **4g**. This is consistent with the higher inductive electron-withdrawing action of the –O– linkage (aryl-OCF_3), which lessens shielding at the fluorine sites.

All the synthesized thiazole-based hydrazone derivatives (**4a–4n**) were confirmed by high-resolution mass spectrometry (HRMS) using ESI mode. The experimentally observed $[M + H]^+$ peaks showed excellent agreement with the calculated monoisotopic masses, validating the proposed molecular formulae. The **4a** displayed a molecular ion peak at *m*/*z* 360.0404, closely matching the calculated value of 360.0402. Similarly, compounds bearing halogen substituents, such as **4b**, **4h**, **4j**, and **4m**, exhibited characteristic isotope peaks. Compound **4b** (4-chlorophenyl derivative) exhibited an $[M + H]^+$ peak at *m*/*z* 349.0156, closely matching the calculated value of 349.0162, along with a corresponding $(M + H + 2)^+$ peak at *m*/*z* 351.0126, indicative of the natural isotopic abundance of ^{35}Cl and ^{37}Cl. Similarly, **4m**, bearing a 3-chlorophenyl group, displayed a strong $[M + H]^+$ peak at *m*/*z* 349.0153, again consistent with its calculated mass. Compound **4j**, a dichlorinated derivative (3,4-dichlorophenyl), presented a characteristic triplet isotopic distribution with peaks at *m*/*z* 382.9766, 384.9737, and 386.9712, reflecting the presence of two chlorine atoms with combinations of $^{35}Cl/^{35}Cl$, $^{35}Cl/^{37}Cl$, and $^{37}Cl/^{37}Cl$. The brominated compound **4h** (4-bromophenyl derivative) showed an $[M + H]^+$ peak at *m*/*z* 392.9657 and a corresponding $(M + H + 2)^+$ peak at *m*/*z* 394.9631, consistent with the typical 1 : 1 isotopic pattern of ^{79}Br and ^{81}Br. The isotopic intensity ratio for monochlorinated compounds is found to be approximately 3 : 1, while for dichlorinated compound is approximately 9 : 6 : 1. Compounds **4f** and **4g**, containing trifluoromethyl and trifluoromethoxy groups, respectively, also showed matching calculated and observed values (*m*/*z* 383.0425 and 399.0376). All other compounds also showed a very good match with the expected mass values. The close correspondence between calculated and observed masses for all derivatives strongly supports the successful synthesis and molecular integrity of the target compounds.

3.2. Evaluation of *in vitro* antitubercular activity of synthesized compounds

The synthesized furan–thiazole hydrazone derivatives (**4a–4n**) were screened for antitubercular activity against *Mycobacterium tuberculosis* H37Rv strain (ATCC 27294), and their minimum inhibitory concentrations (MICs) were determined. The results are given in Table 1. The graphical representation is given Fig. S1 and MIC in micro molar concentration Table S1. The MIC values ranged from 3.12 to 12.5 μg mL^{-1}, indicating varying degrees of efficacy depending on the nature and position of the substituents on the aryl ring attached to the thiazole moiety. Compounds **4a**, **4b** and **4c** demonstrated the most promising activity, with MIC values of 3.12 μg mL^{-1}, which is on par with the standard drug pyrazinamide (MIC = 3.12 μg mL^{-1}) and less effective than standard drugs like isoniazid and ethambutol (both MIC = 1.6 μg mL^{-1}). Compound **4a**, which

Table 1 Antitubercular activity of synthesized compounds (**4a–4n**) against *Mycobacterium tuberculosis* (H37 RV strain): ATCC no. 27294

Compound	MIC (μg mL^{-1})
4a	3.12
4b	3.12
4c	3.12
4d	6.25
4e	6.25
4f	6.25
4g	12.5
4h	6.25
4i	12.5
4j	12.5
4k	6.25
4l	6.25
4m	12.5
4n	6.25
Isoniazid	1.6
Ethambutol	1.6
Pyrazinamide	3.12
Rifampicin	0.8
Streptomycin	0.8

bears both a 4-nitrophenyl and a 5-nitrofuran group, showed significant activity, suggesting a synergistic enhancement from the presence of two strong electron-withdrawing nitro groups. Similarly, **4b**, with a 4-chlorophenyl substituent, also exhibited high activity, further confirming the positive influence of electron-withdrawing groups at the *para*-position. Compound **4c**, incorporating a *p*-tolyl group (a weak electron-donating methyl group), maintained comparable activity. The compound **4d** which carries a *p*-methoxyphenyl substituent, and **4e**, with a bulky naphthyl group, both showed decreased activity with MIC values of 6.25 μg mL^{-1}. Furthermore, compounds **4f** and **4g**, featuring trifluoromethyl and trifluoromethoxy substituents respectively, displayed further diminished activity (MIC = 6.25 and 12.5 μg mL^{-1}). Although fluorine-containing groups typically enhance bioavailability and metabolic stability, in these cases, negatively impact interaction with the biological target. The role of halogen atoms was further examined through compound **4h** (4-bromophenyl), which retained moderate activity (MIC = 6.25 μg mL^{-1}), indicating that bulky halogens like bromine can still show reasonable activity. On the other hand, **4j** with a 3,4-dichlorophenyl group exhibited reduced activity (MIC = 12.5 μg mL^{-1}), pointing to the importance of substitution pattern—*para*-substitution being more favorable than *meta*- or multi-substitution due to its effect on electronic distribution and steric profile. Compound **4i**, bearing an unsubstituted phenyl ring, also showed low activity (MIC = 12.5 μg mL^{-1}), suggesting that the presence of a substituent is critical for effective interaction with the target site. The derivatives **4k**, **4l**, and **4n** incorporate extended conjugation through an additional aromatic linker with polar functionalities such as phenol and nitrile groups. These compounds showed intermediate activity (MIC = 6.25 μg mL^{-1}). Finally, compound **4m**, which features a 3-chlorophenyl group, was among the least active (MIC = 12.5 μg mL^{-1}), underscoring that substitution at the *meta*-position of chloro group is less favorable for biological activity compared to its *para*-counterpart.

3.3. *In vitro* antibacterial activity evaluation of synthesized compounds

The antimicrobial evaluation of the synthesized furan–thiazole hydrazone derivatives (**4a–4n**) was carried out against *Staphylococcus aureus* (ATCC 23235) and *Escherichia coli* (ATCC 25922) using the Kirby–Bauer disk diffusion method, followed by MIC determination *via* the microbroth dilution method for active compounds. Out of the fourteen synthesized derivatives, some of the compounds exhibited measurable zones of inhibition, indicating antibacterial potential. Compounds **4c**, **4d**, **4f**, **4g**, **4k**, **4l**, and **4m** were found to be active against *S. aureus*, with inhibition zones ranging from 9 to 19 mm (Table 2). Among these, compound **4g** exhibited the highest activity against *S. aureus* (19 mm) and also showed notable activity against *E. coli* (17 mm). Compound **4f** also displayed dual antibacterial activity with inhibition zones of 16 mm (*S. aureus*) and 12 mm (*E. coli*). The MIC values (μg mL^{-1}) of the active compounds further supported these findings (Table 2). MIC in μM is given Table S2.

Table 2 Antibacterial activity of synthesized compounds (**4a–4n**) against *Staphylococcus aureus* (ATCC 23235) and *Escherichia coli* (ATCC 25922)

	Zone of inhibition in mm (MIC in μg mL^{-1})	
Compounds	*Staphylococcus aureus* ATCC 23235	*Escherichia coli* ATCC 25922
4a	00	00
4b	00	00
4c	10 (512)	00
4d	11 (512)	00
4e	00	00
4f	16 (512)	12 (256)
4g	19 (256)	17 (512)
4h	00	00
4i	00	00
4j	00	00
4k	10 (512)	00
4l	13 (512)	10 (512)
4m	9 (512)	00
4n	00	00
Tetracycline	13 (4)	10 (8)

Compounds **4c**, **4d**, **4f**, **4k**, **4l**, and **4m** showed MICs of 512 μg mL^{-1} against *S. aureus*, while compound **4g** demonstrated better potency with a MIC of 256 μg mL^{-1}. For *E. coli*, compound **4f** had the lowest MIC value (256 μg mL^{-1}), followed by **4g** and **4l** (512 μg mL^{-1}). The rest of the compounds, including **4a**, **4b**, **4e**, **4h**, **4i**, **4j**, and **4n**, were found to be inactive against both bacterial strains, showing no zone of inhibition. Compared to the standard drug tetracycline, which showed inhibition zones of 13 mm (*S. aureus*) and 10 mm (*E. coli*), compounds **4f** and **4g** displayed comparable or superior activity, especially against *S. aureus*. These results suggested that groups such as trifluoromethyl (**4f**) and trifluoromethoxy (**4g**) enhances antibacterial activity in this series. The structure–activity relationship (SAR) analysis of the synthesized furan–thiazole hydrazone derivatives (**4a–4n**) revealed that the nature and position of substituents on the phenyl ring significantly influence antibacterial activity. Compounds **4f** and **4g** showed the highest activity against both *S. aureus* and *E. coli*. Notably, **4g**, containing a trifluoromethoxy substituent, exhibited the largest zone of inhibition (19 mm against *S. aureus*) and the lowest MIC (256 μg mL^{-1}), indicating superior potency. Compounds with electron-donating groups such as methoxy (**4d**) and methyl (**4c**) displayed moderate activity against *S. aureus*, but were inactive against *E. coli*, implying that such substitutions may restrict spectrum of action. Additionally, the presence of halogen atoms like chlorine (**4m**) and hydroxyl (**4k**) contributed to marginal activity, suggesting a minor role in antibacterial enhancement. In contrast, compounds with unsubstituted phenyl rings or bulkier groups such as naphthyl (**4e**) or dichlorophenyl (**4j**) were completely inactive, highlighting the importance of electronic and steric effects in modulating antibacterial activity. This SAR findings suggest that introduction of strong electron-withdrawing substituents at the *para* position of the aryl ring is crucial for improved activity in this series.

3.4. Molecular docking analysis

3.4.1. Docking on cytochrome P450 14α-sterol demethylase. Cytochrome P450 14α-sterol demethylase (CYP51) is a key enzyme in the sterol biosynthesis pathway, responsible for the demethylation of sterol precursors—a critical step in the production of functional sterols necessary for maintaining cellular membrane structure and fluidity. This enzyme is highly conserved across multiple species, including fungi and

Table 3 Interacting residues for all compounds inside the binding cavity of target CYP51

Molecule	Affinity (kcal mol^{-1})	Hydrophobic interactions	Halogen	H-bonding interactions	van der Waals
4a	−10.69	Ala256(4.13, 5.10); Cys394(3.55); Thr260(3.78); His259(5.36); Val434(5.44); Phe78(4.92); Tyr76(4.75); Leu321(4.58)(5.14);			
4b	−10.76	Phe78(5.02); Tyr76(5.19); Leu321(4.92, 5.36, 5.37); His259(4.53); Ala256(4.01, 5.03); Phe387(4.82); Ala400(4.21); Thr260(4.81); Cys394(3.49); Val434(5.36)			
4c	−10.32	His259(5.12); Phe78(5.00); Val434(5.24); Leu321(3.89, 4.56); Ala256(5.37); Phe387(4.71); Ala400(4.42); Cys394(3.47); Thr260(3.665)			
4d	−8.53	Val434(5.34); His259(5.18); Tyr76(4.87); Phe78(4.87); Ala256(4.04, 5.19); Leu321(4.52, 5.10); Thr260(83.75); Cys394(3.56); Pro320(4.00); Phe387(4.67)			
4e	−9.3	Phe78(5.07); His259(5.14); Leu321(4.51); Val434(5.36); Ala256(3.90, 4.74); Thr260(4.13); Cys394(3.50); Pro320(4.93); Ala400(5.50)			Gly257
4f	−9.27	Cys394(4.74); Val395(5.09); Ala256(3.83); Met79(4.75, 5.28); Phe78(5.16); Leu321(4.34, 5.21)	Met433 (2.61, 3.20)	Val434(4.88); His259(3.49); His101(3.51)	
4g	−7.64	Tyr76(4.90); Ala256(4.06); Pro320(3.82); Phe387(4.66); His259(5.16); Leu321(4.55, 4.92); Phe78(4.99)	pro386(3.12)	Thr264(3.57); Thr260(3.46); Cys394(3.94)	
4h	−9.21	Tyr76(4.71); Ala256(4.20)(5.07); His259(5.28); Val434(5.43); Phe78(5.01); Leu321(4.50)(5.12); Cys394(2.88)(3.57)(4.81); Thr260(3.78); Phe387(4.69)			
4i	−4.76	Phe387(4.83); Cys394(3.53)(3.60)(4.94); Thr260(3.86); Tyr76(4.61); His259(5.38); Phe78(4.93); Cal434(5.45); Leu321(4.55)(5.25); Ala256(4.23)(4.92)			Gly257
4j	−4.32	Val434(5.39); Phe78(5.06); His259(5.12); Ala256(5.16); Leu321(3.98); Cys394(3.63)		Thr260(3.17)	
4k	−8.76	Ala256(4.39); Leu321(4.74); Tyr76(5.17); Cys394(3.62)			
4l	−8.69	Phe78(4.98); Ty76(5.28); Leu321(4.77); Val434(5.42); His259(4.54); Ala256(4.12, 4.95); Thr260(3.78); Cys394(3.50)			
4m	−5.32	Phe78(5.03); His259(5.14); Tyr76(4.83); Met433(4.96); Val434(5.39); Leu321(3.99); Cys394(3.17)		Thr260(3.62)	
4n	−8.53	Leu321(3.94); Cys394(3.66); Phe78(4.98); Ala256(5.14)		Ile323(2.56)	
Cocrystal ligand	−8.69	Tyr76(3.71); Phe78(5.30); Met79(5.48); Leu321(3.83)			
Isoniazid	−9.01	Cys394(5.10); Pro320(4.64); Ala400(4.92); Thr260(3.72); Phe387(4.64)		Pro386(2.14)	

Table 4 2D and 3D interaction diagrams of compounds **4a**, **4b**, **4c** and isoniazid against target CYP51

Compound	2D interaction diagram	3D interaction diagram
4a	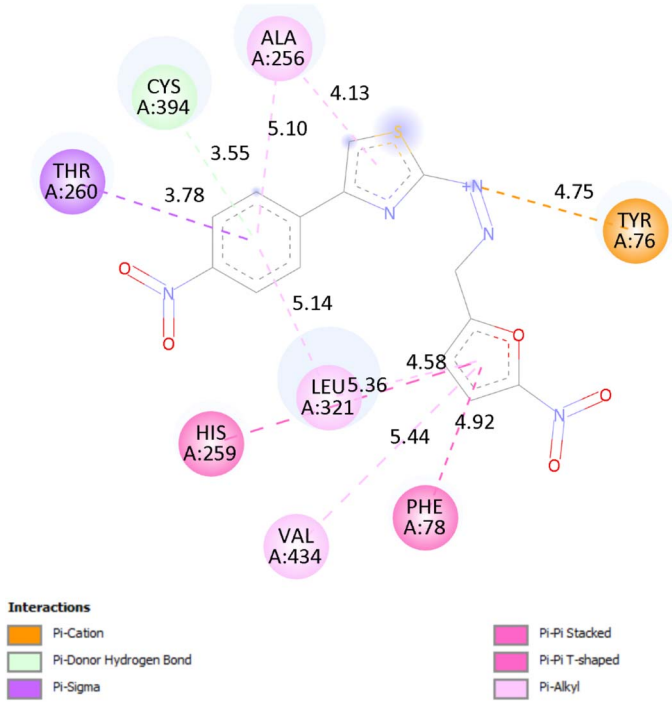	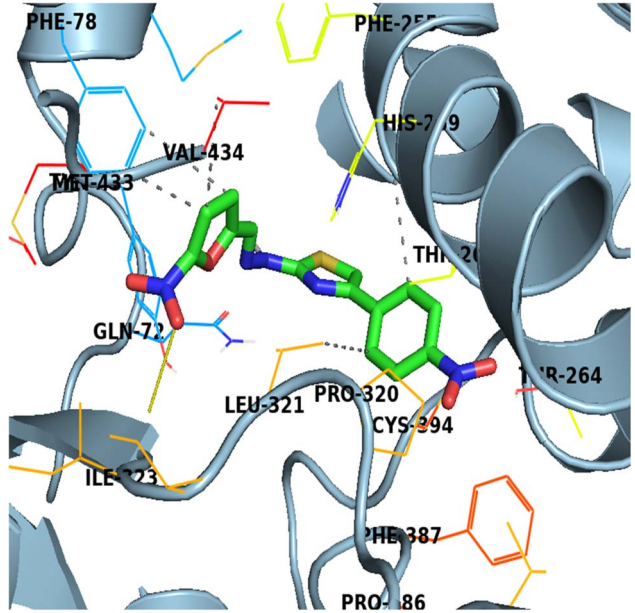

Table 4 (*Contd.*)

Compound	2D interaction diagram	3D interaction diagram
4b	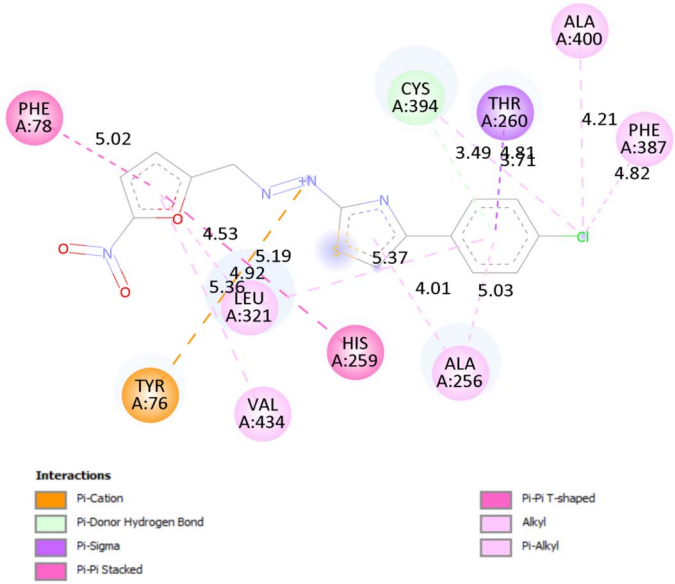	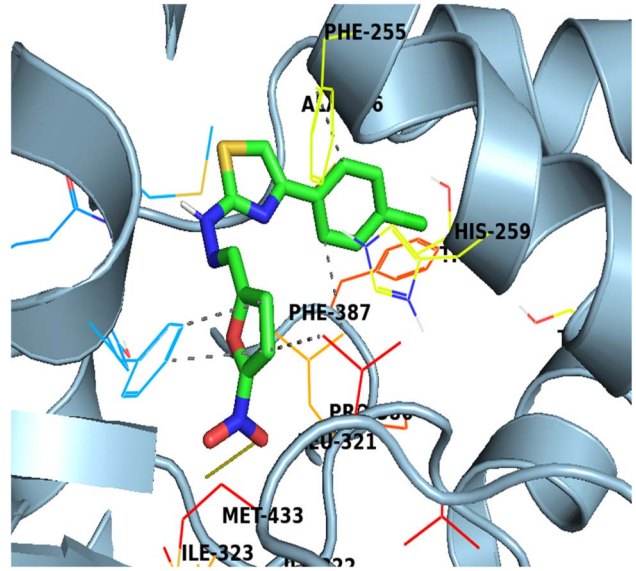

Table 4 (*Contd.*)

Compound	2D interaction diagram	3D interaction diagram
4c	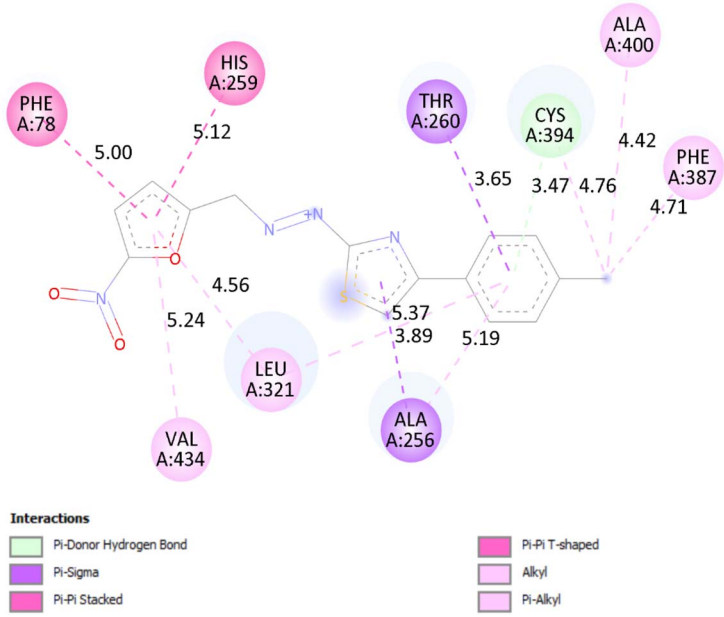	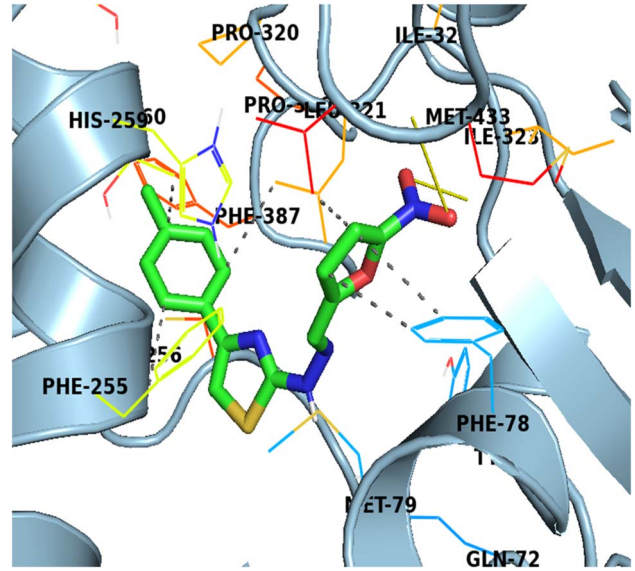

Table 4 (*Contd.*)

Compound	2D interaction diagram	3D interaction diagram
Isoniazid	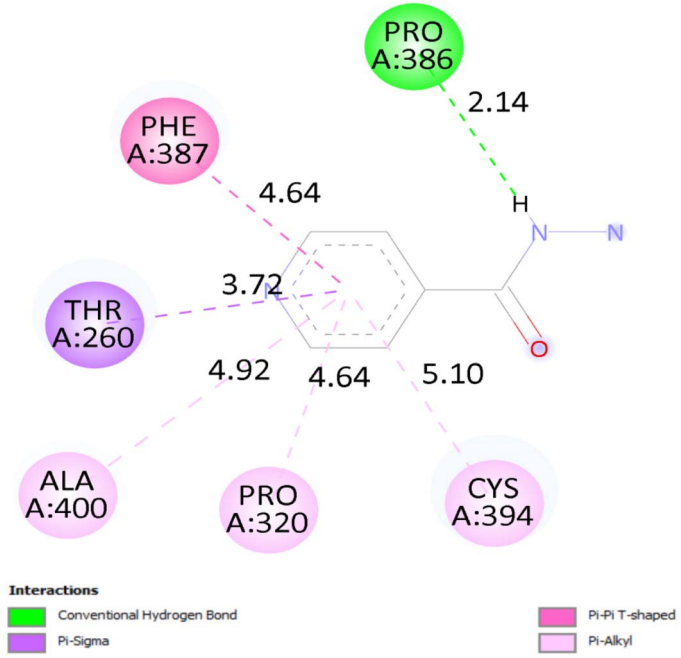	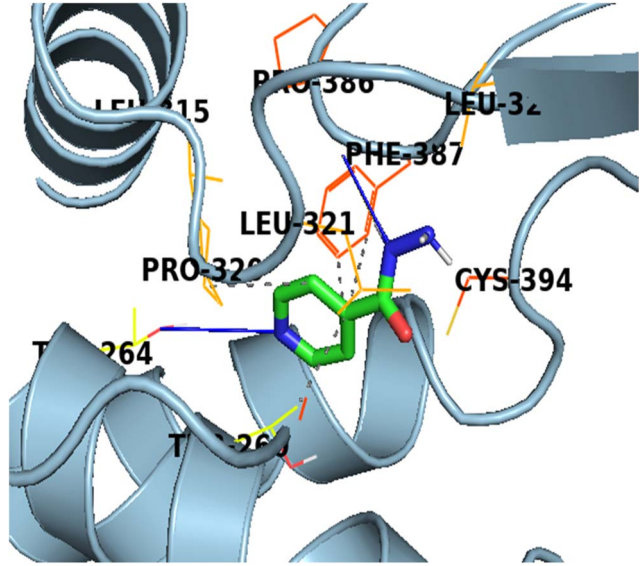

Mycobacterium tuberculosis, making it an attractive and well-validated therapeutic target.[58,77] Inhibition of CYP51 disrupts sterol synthesis, leading to compromised membrane integrity and ultimately cell death. Given its vital role in *M. tuberculosis* survival, CYP51 is considered a promising target for developing new antitubercular agents, especially in the context of increasing drug resistance.[78] The molecular docking results of compounds **4a–4n** using AutoDockTool includes binding affinities, docking scores, and interaction profiles which are summarized in Table 3. The 2D and 3D interaction diagrams of selected compounds with CYP51, highlighting key binding interactions, are presented in Table 4. Among the series of furan–thiazole hydrazones docked against *Mycobacterium tuberculosis* CYP51, compounds **4a** (−10.69 kcal mol^{-1}), **4b** (−10.76 kcal mol^{-1}), and **4c** (−10.32 kcal mol^{-1}) exhibited the strongest binding affinities compared to the co-crystalized ligand (−8.69 kcal mol^{-1}) and isoniazid (−9.01 kcal mol^{-1}). Compound **4a** showed favorable binding within the active site, interacting with Ala256 (4.13, 5.10 Å), Cys394 (3.55 Å), Thr260 (3.78 Å), His259 (5.36 Å), Val434 (5.44 Å), Phe78 (4.92 Å), Leu321 (4.58 Å and 5.14 Å); and Tyr76 (4.75 Å), suggesting a stable complex through hydrophobic interactions. Compound **4b** exhibited stable binding by interacting with key residues including Phe78 (5.02 Å), Tyr76 (5.19 Å), Leu321 (4.92, 5.36, 5.37 Å), His259 (4.53 Å), Ala256 (4.01, 5.03 Å), Phe387 (4.82 Å), Ala400 (4.21 Å), Thr260 (4.81 Å), Val434 (5.36 Å); and Cys394 (3.49 Å), indicating a strong binding affinity through hydrophobic contacts. Isoniazid displayed hydrophobic interactions with Cys394, Pro320, Ala400, Phe387, and Thr260 and formed hydrogen bond with and Pro386, indicating stable binding within the active site. The overlapping interaction profiles of the top candidates with those of the control and reference drugs highlight their potential as promising inhibitors of CYP51 and worthy candidates for further antitubercular development.

3.4.2. Docking on common antibacterial target. 2,2-Dialkylglycine decarboxylase (DGD) is a key enzyme in bacterial metabolism that catalyzes the decarboxylation of 2,2-dialkylglycines to produce amines and acetate. It plays an important role in amino acid degradation, enabling bacteria to utilize alternative carbon sources, especially under nutrient-limited conditions. By supporting metabolic processes, DGD aids bacterial adaptation to diverse environments, including host tissues, thereby enhancing survival and virulence. Thus, targeting DGD is considered as an important target in developing newer antibacterials. Thus, we carried out docking analysis of synthesized compounds (**4a–4n**) against 2,2-dialkylglycine decarboxylase (PDB id: 1d7u) (Table 5). The 2D and 3D interaction diagrams of selected compounds (**4f** and **4g**) with CYP51,

Table 5 Docking interaction analysis for a series of furan–thiazole hydrazones (**4a–4n**) against 2,2-dialkylglycine decarboxylase (PDB id: 1d7u)

Molecules	Affinity (kcal mol^{-1})	Hydrophobic interactions (distance, Å)	Halogen	H-bonding interactions (distance, Å)
4a	−4.56	Trp138(4.51, 4.73, 4.94); Ala245(3.99)	—	Lys272(3.55); Gln246(2.98)
4b	−4.99	Ala112(4.83); Gly11(3.99)	—	Trp138(3.04, 3.25); Ser215(2.80); Gln246(3.00, 3.07); Arg406(3.21); Lys272(3.37); Ser54(3.10)
4c	−6.88	Trp138(4.48, 4.76, 5.01); Ala245(3.95)	—	Gln246(2.99); Lys272(3.55)
4d	−7.39	Ala245(3.95); Trp138(4.53, 4.77, 4.99); Val396(4.54)	—	Gln246(2.97); Lys272(3.57)
4e	−3.91	Arg406(4.15); Trp138(4.62, 4.96, 5.00); Val396(4.64); Ala245(4.05)	—	Gln246(2.95)
4f	−7.89	Ala245(4.21)	—	Gln246(2.92); Trp138(3.34); Lys272(3.52)
4g	−9.65	Ala152(4.45); Trp138(4.64, 4.76, 4.79); Ala245(3.93)	Ser215(3.36)	Gln246(2.93); Lys272(3.62)
4h	−3.77	Trp138(4.51, 4.75, 5.00); Ala245(3.96)	—	Gln246(2.99); Lys272(3.55)
4i	−3.86	Arg(4.05); Val396(4.10); Trp138(4.51, 4.84, 4.96, 5.01); Ala245(3.87)	—	Gln246(2.98); Lys272(3.66)
4j	−3.33	Ala245(4.18); Thr110(3.60)	—	Gly111(3.14); Ala112(2.96); Gln246(2.80); Trp138(3.32); Lys272(3.61)
4k	−6.59	Trp138(4.68); Ala245(4.03)	—	Ser271(2.85); Leu280(1.92); Lys272(4.62); Gln246(3.03)
4l	−7.42	Ala245(3.91); Trp138(4.44, 4.80, 4.91)	—	Gln246(2.98); Lys272(3.56)
4m	−6.21	Trp138(4.61, 4.78, 5.04); Val396(4.25); Ala245(4.07)	—	Gln246(3.00)
4n	−2.94	Ala245(4.17); Thr110(3.80)		Ser109(2.34); Gly111(3.36); Lys272(3.74); Trp138(3.30); Gln246(2.80); Ala112(2.94)
Control (co-crystal)	−7.61	—		Asn115(2.80); Asp243(2.08); Gly111(3.00); Trp138(3.07); Ser215(2.47, 3.10); Gln246(3.10)

Table 6 2D and 3D interaction diagrams of compounds **4f** and **4g** against target 1d7u

Compound	2D interaction diagram	3D interaction diagram
4f	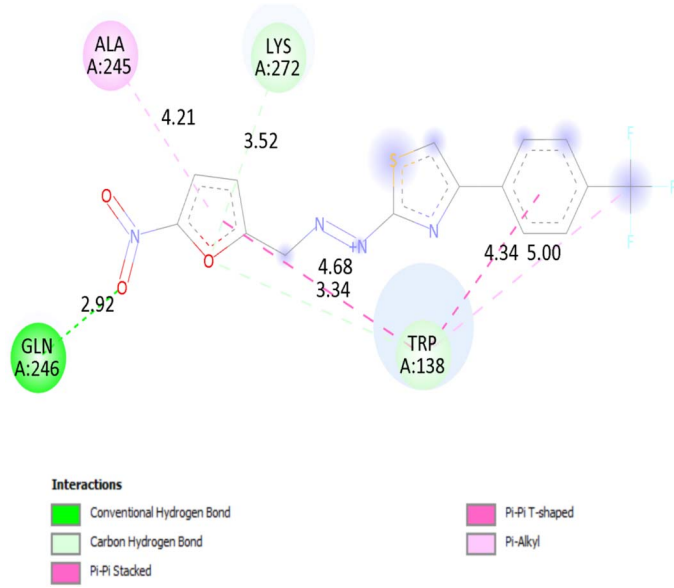	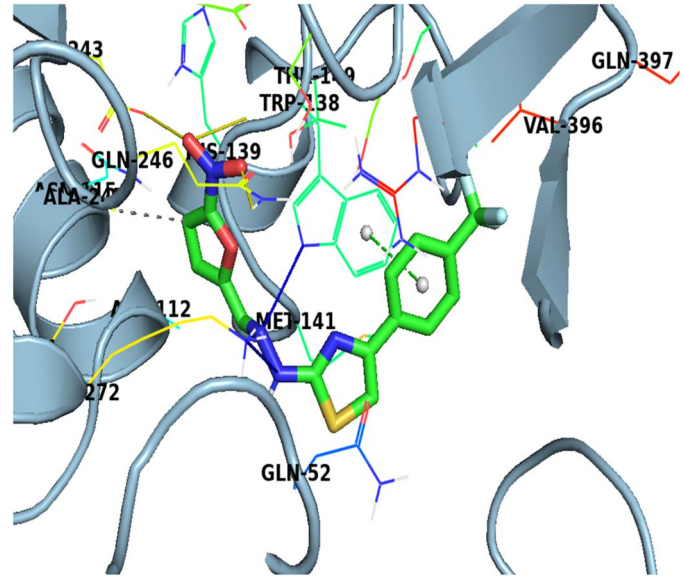

Table 6 (*Contd.*)

Compound	2D interaction diagram	3D interaction diagram
4g	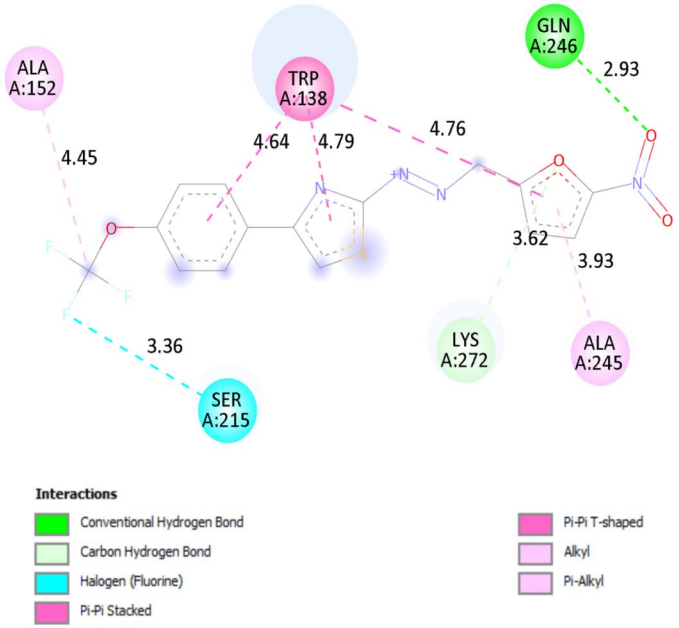	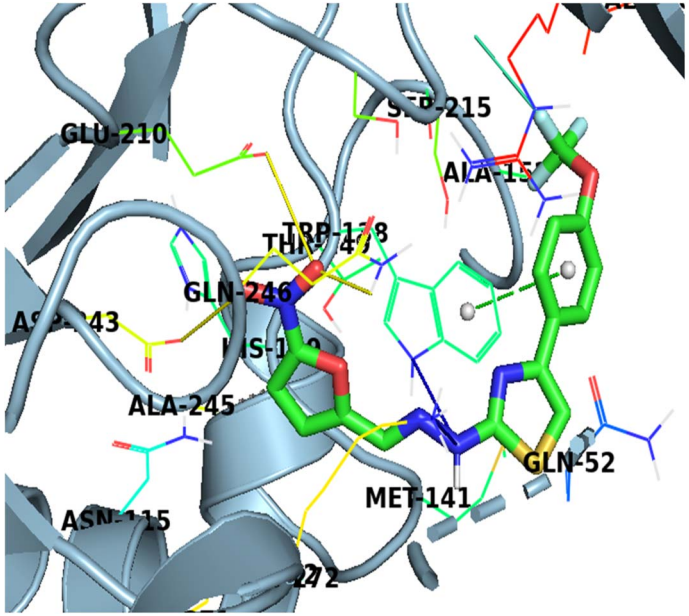

Table 7 *In silico* ADME properties for synthesized compounds as calculated by 'SwissADME'

Molecule	MW	#Heavy atoms	#Aromatic heavy atoms	Lipinski #violations	Ghose #violations	Veber #violations	Egan #violations	Muegge #violations
4a	359.32	25	16	0	0	1	1	1
4b	348.76	23	16	0	0	0	0	0
4c	328.35	23	16	0	0	0	0	0
4d	344.35	24	16	0	0	0	1	0
4e	364.38	26	20	0	0	0	0	1
4f	382.32	26	16	0	1	0	0	1
4g	398.32	27	16	0	1	0	1	1
4h	393.22	23	16	0	0	0	0	0
4i	314.32	22	16	0	0	0	0	0
4j	383.21	24	16	0	0	0	0	1
4k	330.32	23	16	0	0	1	1	0
4l	339.33	24	16	0	0	1	1	0
4m	348.76	23	16	0	0	0	0	0
4n	330.32	23	16	0	0	1	1	0

Molecule	GI absorption	BBB permeant	Pgp substrate	CYP1A2 inhibitor	CYP2C19 inhibitor	CYP2C9 inhibitor	CYP2D6 inhibitor	CYP3A4 inhibitor
4a	Low	No	No	Yes	Yes	Yes	No	Yes
4b	Low	No	No	Yes	Yes	Yes	No	No
4c	High	No	No	Yes	Yes	Yes	No	No
4d	Low	No	No	Yes	Yes	Yes	No	No
4e	Low	No	No	Yes	Yes	Yes	No	No
4f	Low	No	No	Yes	Yes	Yes	No	No
4g	Low	No	No	Yes	Yes	Yes	No	No
4h	Low	No	No	Yes	Yes	Yes	No	No
4i	High	No	No	Yes	Yes	Yes	No	No
4j	Low	No	No	Yes	Yes	Yes	No	No
4k	Low	No	No	Yes	Yes	Yes	No	No
4l	Low	No	No	Yes	Yes	Yes	No	No
4m	Low	No	No	Yes	Yes	Yes	No	No
4n	Low	No	No	Yes	Yes	Yes	No	No

highlighting key binding interactions, are presented in Table 6. Among the series of furan–thiazole hydrazones (**4a–4n**) docked against 2,2-dialkylglycine decarboxylase (PDB ID: 1d7u), compound **4g** exhibited the highest binding affinity with a docking score of −9.65 kcal mol^{-1}, surpassing the co-crystal ligand (control), which showed an affinity of −7.61 kcal mol^{-1}. Compound **4g** formed strong hydrophobic interactions with key residues such as Trp138, Ala245, and Ala152, and was further stabilized by a halogen bond with Ser215 (3.36 Å), along with hydrogen bonds involving Gln246

Table 8 *In silico* toxicity properties for synthesized compounds as calculated by 'ADMETlab 2.0' (https://admetmesh.scbdd.com/)

Compounds	hERG	H-HT	DILI	AMES toxicity	Rat oral acute toxicity	FDAMDD	Skin sensitization	Carcinogenicity	Eye corrosion	Eye irritation	Respiratory toxicity
4a	0.055	0.881	0.979	0.998	0.076	0.526	0.52	0.971	0.133	0.97	0.899
4b	0.011	0.832	0.978	0.99	0.15	0.499	0.254	0.955	0.028	0.946	0.922
4c	0.008	0.889	0.976	0.993	0.117	0.262	0.283	0.96	0.081	0.967	0.914
4d	0.016	0.926	0.976	0.993	0.132	0.417	0.289	0.97	0.04	0.958	0.912
4e	0.012	0.885	0.979	0.994	0.127	0.701	0.243	0.97	0.016	0.962	0.874
4f	0.007	0.905	0.971	0.984	0.175	0.383	0.159	0.941	0.032	0.917	0.95
4g	0.026	0.982	0.984	0.988	0.521	0.665	0.132	0.97	0.004	0.294	0.916
4h	0.011	0.65	0.977	0.98	0.105	0.457	0.328	0.957	0.199	0.973	0.936
4i	0.006	0.881	0.976	0.993	0.258	0.298	0.337	0.959	0.136	0.974	0.933
4j	0.013	0.711	0.977	0.986	0.055	0.668	0.25	0.955	0.025	0.916	0.947
4k	0.007	0.857	0.977	0.989	0.165	0.303	0.292	0.962	0.063	0.966	0.932
4l	0.03	0.952	0.978	0.993	0.273	0.762	0.323	0.967	0.036	0.955	0.94
4m	0.009	0.85	0.975	0.988	0.122	0.664	0.28	0.954	0.056	0.934	0.921
4n	0.008	0.865	0.974	0.987	0.182	0.568	0.323	0.962	0.088	0.959	0.934

(2.93 Å) and Lys272 (3.62 Å). Other high-affinity compounds included **4f** (−7.89 kcal mol^{-1}) and **4l** (−7.42 kcal mol^{-1}), which also interacted consistently with Trp138, Ala245, Gln246, and Lys272—residues critical for ligand binding (Fig. 2). In comparison, the control ligand formed multiple hydrogen bonds, notably with Trp138, Gln246, Ser215, and Asp243, indicating similar binding site preferences. The best binding of **4g** suggests its promising potential as a lead molecule.

3.5. *In silico* ADME and toxicity analysis

The ADME and drug-likeness analysis of the furan–thiazole hydrazones (**4a–4n**) revealed that most compounds exhibit favourable drug-like properties, with no violations of Lipinski's rule, indicating good oral bioavailability potential (Table 7). Compounds **4b**, **4c**, **4h**, **4i**, and **4m** emerged as the most promising candidates, showing zero violations across all five major drug-likeness filters (Lipinski, Ghose, Veber, Egan, and Muegge). The compounds like **4a**, **4e**, **4f**, **4g**, **4j**, **4k**, **4l**, and **4n** showed one or more violations, mostly related to Veber and Muegge rules, which may affect bioavailability or lead-likeness. Regarding ADME properties, only **4c** and **4i** demonstrated high gastrointestinal (GI) absorption, a critical factor for oral drugs, while the remaining compounds had low GI absorption. None of the molecules were predicted to cross the blood–brain barrier (BBB) or act as P-glycoprotein (Pgp) substrates, which is favourable in avoiding CNS side effects and drug efflux issues. Most compounds were predicted to inhibit multiple cytochrome P450 enzymes. The compounds **4b**, **4c**, **4h**, **4i**, and **4m** possessed good balance of drug-likeness and ADME profiles, making them suitable candidates for further development. The *in silico* toxicity assessment (Table 8) of compounds **4a–4n** revealed that all molecules exhibited excellent hERG safety (probability ≤ 0.055), indicating a low risk of cardiotoxicity. However, all compounds showed poor human hepatotoxicity (H-HT) profiles (values > 0.7), and similarly, high DILI probabilities (≥0.971), suggesting significant liver toxicity risk. Most compounds also showed very poor AMES toxicity scores (≥0.98), indicating a strong mutagenic potential. Regarding rat oral acute toxicity, the majority of compounds showed excellent to moderate safety (values mostly < 0.3), with compound **4g** being the least favourable (0.521). FDAMDD predictions showed that the compounds **4c** and **4i** have good safety, while others (**4l** and **4e**) fell in the medium to poor range (>0.7). Skin sensitization values were mostly moderate (0.13–0.52), implying potential for mild sensitization. All compounds showed high carcinogenicity scores (≥0.941), indicating a strong potential carcinogenic risk. Eye corrosion predictions were mostly in the excellent range (<0.2), while eye irritation values were generally poor (>0.9), suggesting a notable risk of ocular irritation.

3.6. DFT study

3.6.1. Optimized molecular geometries and electronic parameters. DFT calculations were performed at the B3LYP/6-31G(d,p) level to evaluate the geometric and electronic properties of the synthesized furan–thiazole hydrazone derivatives (**4a–4n**) and to understand their structure–activity relationships with respect to antitubercular potential. The optimized molecular structures (Fig. 3) revealed predominantly non-planar conformations with extended π-conjugation, influenced by the nature of the substituents present on the phenyl or heteroaryl rings.

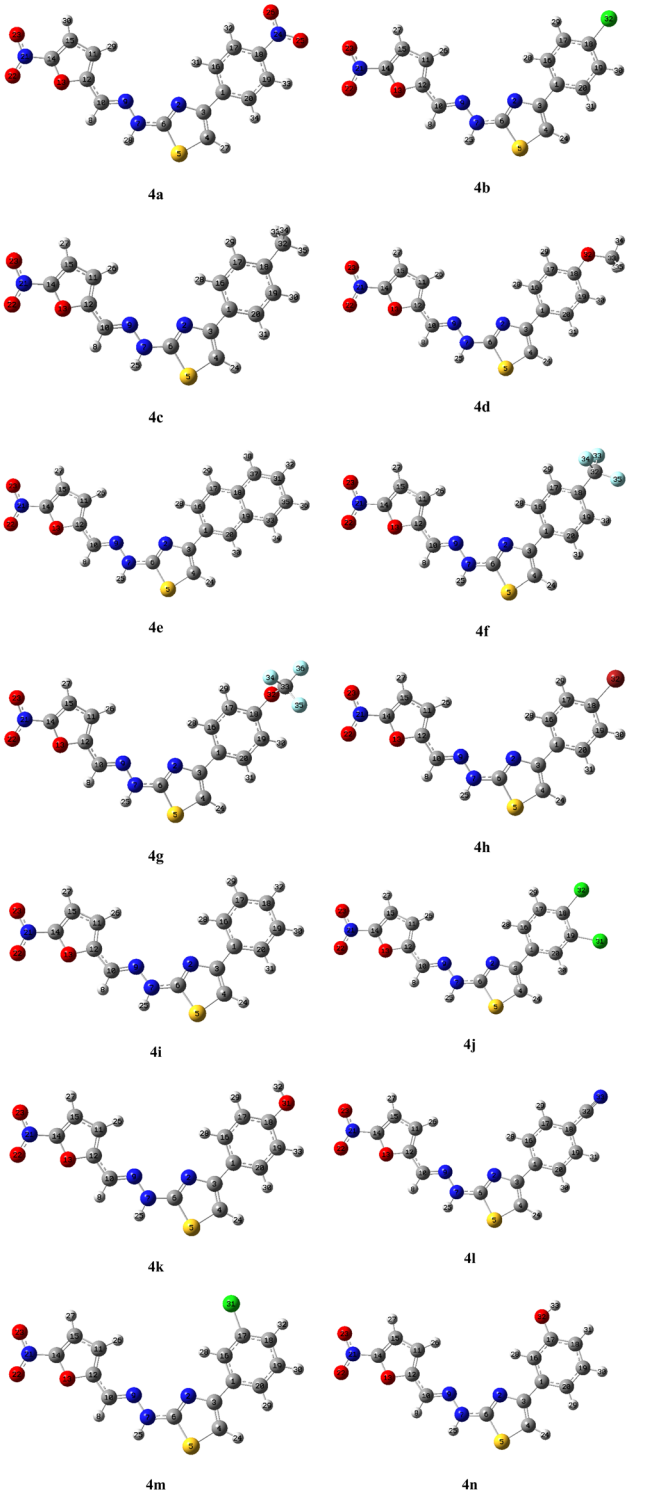

Fig. 3 Optimized structures of synthesized derivatives.

Table 9 Electronic parameters of the synthesized compound (**4a–4n**)

Entry	E (a.u.)	E_{HOMO} (eV)	E_{LUMO} (eV)	I (eV)	A (eV)	E_g (eV)	Dipole moment (debye)
4a	−1584.72	−4.10	−2.88	4.10	2.88	3.22	4.3933
4b	−1841.82	−5.81	−2.74	5.81	2.74	3.05	5.3810
4c	−1421.54	−5.41	−2.47	5.41	2.47	2.94	4.0941
4d	−1494.75	−5.43	−2.44	5.43	2.44	2.79	7.5059
4e	−1535.87	−5.57	−2.70	5.57	2.70	2.87	5.8847
4f	−1719.24	−5.93	−2.80	5.93	2.80	3.13	5.5299
4g	−1794.48	−5.87	−2.78	5.87	2.78	3.09	5.4229
4h	−3953.33	−5.80	−2.74	5.80	2.74	3.04	5.3859
4i	−1382.22	−5.49	−2.49	5.49	2.49	3.00	5.8882
4j	−2301.41	−5.93	−2.83	5.93	2.83	3.1	4.0109
4k	−1457.44	−5.49	−2.48	5.49	2.48	2.81	4.9547
4l	−1474.44	−403	−2.84	4.03	2.84	3.17	4.2818
4m	−1841.82	−5.84	−2.74	5.84	2.74	3.10	4.9542
4n	−1457.44	−5.44	−2.45	5.44	2.45	2.99	4.8454

To gain deeper insight into their electronic behaviour, the electronic parameters (Table 9) such as frontier molecular orbitals (FMOs), energy gaps (E_g), dipole moments, and global reactivity descriptors (Table 10) were analysed and correlated with the observed biological activity. The HOMO and LUMO energy levels, which provide insight into a molecule's electron-donating and accepting capacities [80] exhibited significant variation across the series, reflecting the effect of different substituents. The pictorial representation of HOMO–LUMO plots are given in Table S3. HOMO energies ranged from −4.10 eV (**4a**) to −5.93 eV (**4f** and **4j**), while LUMO energies spanned −2.44 eV (**4d**) to −2.88 eV (**4a**). Consequently, the HOMO–LUMO energy gaps varied between 2.79 and 3.22 eV, indicating differences in chemical reactivity and electronic flexibility among the derivatives. Compounds with lower E_g values and higher chemical softness, such as **4c** (E_g = 2.94 eV, softness = 0.68 eV^{-1}) and **4d** (E_g = 2.79 eV, softness = 0.67 eV^{-1}), displayed enhanced electronic polarizability, which typically favours biological interactions. These compounds demonstrated moderate antitubercular activity with MIC values of 3.12–6.25 μg mL^{-1}, suggesting that reduced energy gaps and increased softness can contribute to improved biological response. Interestingly, compounds **4a** and **4b**, bearing electron-withdrawing nitro and chloro substituents, showed the most potent antitubercular activity (MIC = 3.12 μg mL^{-1}) despite relatively higher E_g values (3.22 and 3.05 eV, respectively). This observation indicates that, beyond energy gap considerations, substituent-induced electronic effects play a crucial role in facilitating favourable interactions with the biological target, possibly through enhanced molecular polarity and electrophilicity. This is supported by their high electrophilicity indices (ω = 9.98 eV for **4a** and 5.95 eV for **4b**) and significant dipole moments (4.39 and 5.38 debye), which can enhance binding affinity toward enzyme active sites or receptor proteins. In contrast, derivatives such as **4f**, **4j**, and **4m** exhibited lower biological activity (MIC = 12.5 μg mL^{-1}), which can be attributed to their higher energy gaps (3.10–3.13 eV). These structural features likely reduce their ability to participate effectively in non-covalent interactions critical for biological activity. The observed trends were further supported by global reactivity descriptors, where higher electronegativity (χ) and electrophilicity (ω) values were generally associated with compounds exhibiting better antitubercular efficacy. For instance, **4a** showed a high electrophilicity index (ω = 9.98 eV) and low hardness (η = 0.61 eV), consistent with its excellent activity profile. Moreover, dipole moments across the series ranged from 4.01 to 7.51 debye, with higher values in compounds such as **4d** (7.51 D) reflecting enhanced molecular polarity, which may contribute to favorable interactions with the polar environment of the mycobacterial target. Additionally, compounds with higher maximum electronic charge transfer values (ΔN_{max}), such as **4a** (5.72 eV) and **4l** (5.77 eV), demonstrated increased softness and electron accommodation capacity, features that support effective biological engagement. The DFT derived electronic parameters revealed that electron-withdrawing or donating groups significantly affect the electronic distribution, reactivity, and polarity of the compounds, which correlates with their antitubercular activity. The study

Table 10 Global reactivity parameters of synthesized compounds[a]

Entry	χ (eV)	η (eV)	σ (eV^{-1})	ω (eV)	μ (eV)	ΔN_{max} (eV)
4a	3.49	0.61	1.64	9.98	−3.49	5.72
4b	4.27	1.53	0.65	5.95	−4.27	2.78
4c	3.94	1.47	0.68	5.28	−3.94	2.68
4d	3.93	1.49	0.67	5.18	−3.93	2.63
4e	4.13	1.43	0.70	5.96	−4.13	2.88
4f	4.36	1.56	0.64	6.09	−4.36	2.79
4g	4.32	1.54	0.65	6.05	−4.32	2.80
4h	4.27	1.53	0.65	5.96	−4.27	2.79
4i	3.99	1.50	0.67	5.31	−3.99	2.66
4j	4.38	1.55	0.65	6.19	−4.38	2.82
4k	3.98	1.50	0.66	5.27	−3.98	2.65
4l	3.43	0.59	1.68	9.91	−3.43	5.77
4m	4.29	1.55	0.64	5.94	−4.29	2.77
4n	3.94	1.49	0.67	5.20	−3.94	2.64

[a] χ = electronegativity; η = chemical hardness; σ, chemical softness; ω, global electrophilicity; μ, chemical potential; ΔN_{max} = maximum electronic charge.

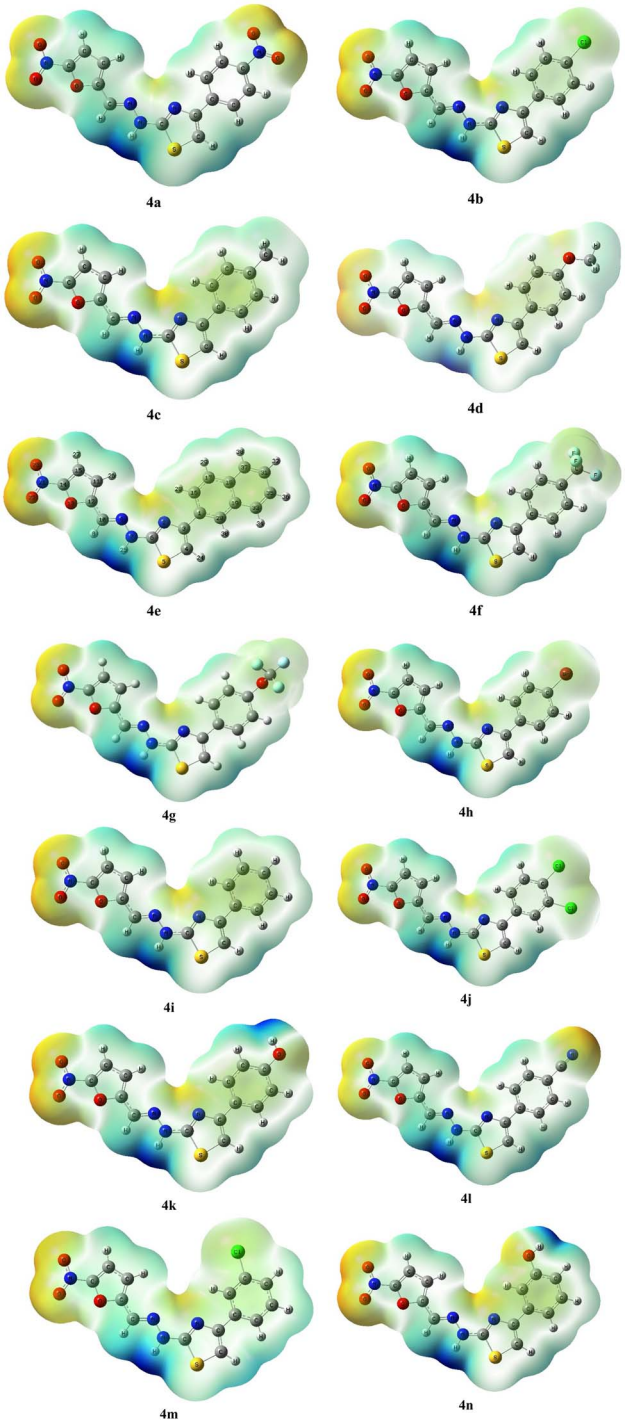

Fig. 4 Molecular electrostatic potential (**4a–4n**).

supports the structure–activity relationship and highlights the role of electronic factors in influencing biological efficacy.

3.6.2. Molecular electrostatic potential surface analysis. Molecular Electrostatic Potential (MEP) surface analysis provides a detailed visualization of the charge distribution across a molecule and is an essential computational tool for identifying reactive sites.[79] By projecting the electrostatic potential derived from electron density onto the molecular van der Waals surface, MEP maps offer a three-dimensional, color-coded representation of electronic behavior. In these maps, blue indicates regions of high positive potential (electron-deficient), red denotes areas of negative potential (electron-rich), and yellow signifies zones with moderate negative character. For the synthesized furan–thiazole hydrazone derivatives (**4a–4n**), the MEP surfaces (Fig. 4) clearly illustrate distinct charge separation influenced by the substitution patterns. Intense yellow to red coloration is consistently observed around the oxygen atoms of both the carbonyl and nitro groups, reflecting their high electron density and confirming these atoms as potential nucleophilic centers. This suggests their likely participation in intermolecular interactions such as hydrogen bonding or coordination with electrophiles. Conversely, strong blue regions are prominently localized around the nitrogen atoms particularly those within the hydrazone and thiazole rings indicating significant electron-deficient character.[79] These sites may act as potential acceptors in nucleophilic interactions or hydrogen bond donors, depending on their molecular environment. The MEP distribution demonstrates how specific substituents and heteroatoms modulate the molecule's electronic landscape. The gradient from red to blue across the molecular surface highlights the electronic polarization within the structure, helping to predict the molecule's reactivity, non-covalent binding preferences, and interaction sites.[80] These electrostatic characteristics are key to understanding the chemical behavior of the series and are directly influenced by the type and positioning of electron-donating or -withdrawing groups present in each derivative.

4 Conclusion

The present investigation highlights the successful design and evaluation of a novel series of furan–thiazole hydrazone derivatives (**4a–4n**) as dual-action as antitubercular and antibacterial candidates. The compounds were successfully characterized using FT-IR, ^{1}H NMR, ^{13}C{^{1}H} NMR, ^{19}F NMR, and HRMS techniques. Among the synthesized compounds, **4a**, **4b**, and **4c** displayed notable antitubercular activity, comparable to standard drugs. Compound **4g** emerged as a potent candidate in antibacterial assays, demonstrating better antibacterial activity compared to other derivatives which is attributed to its trifluoromethyl substitution. Molecular docking further validated the bioactivity, with high binding affinities aligning with the *in vitro* data. The structure–activity relationships derived from this study offer valuable insights for the rational design of future analogues. Compounds **4b**, **4c**, **4h**, **4i**, and **4m** demonstrated promising ADME properties, reinforcing their potential leads with acceptable drug-like behavior for further development. The DFT analysis, including electronic structure, frontier molecular orbital distribution, and electrostatic potential mapping provided insights into electronic, chemical and biological aspects. These findings validate the furan–thiazole hydrazone scaffold as a promising platform for the development of new antitubercular and antibacterial agents amid rising drug resistance challenges. Further cytotoxicity and selectivity studies are

planned in future work to evaluate the therapeutic safety profile of the most active compounds.

Ethics approval

Not applicable. This research did not involve studies with human participants or animals.

Consent for publication

All authors have read and approved the final manuscript and consent to its publication.

Author contributions

Yuvraj R. Sable: performed the synthesis of target compounds, spectral characterization, antitubercular and antibacterial analysis. Rahul A. Shinde: performed DFT analyses, and contributed to manuscript writing and revisions. Haya Khader Ahmad Yasin: contributed in the writing and editing of the manuscript. Niraj Ghanwate: conducted antibacterial bioassays and contributed to microbiological data interpretation. Suraj N. Mali: performed and interpreted the molecular docking and ADME studies and contributed to computational data analysis. Suresh K. Ghotekar: contributed to structural design, SAR analysis, and literature review. Dhanesh P. Gawari and Dinesh A. Sasane: Assisted in synthesis, purification, and spectral data interpretation. Vishnu A. Adole: conceived and supervised the research problem, coordinated all experimental and computational work, written and finalized the manuscript. All authors reviewed and approved the final version of the manuscript.

Conflicts of interest

The authors declare that they have no known competing financial interests or personal relationships that could have appeared to influence the work reported in this manuscript.

Data availability

All data supporting the findings of this study are included within the article and its SI files. Additional datasets generated and/or analyzed during the current study are available from the corresponding author upon reasonable request.

Supplementary information is available. See DOI: **https://doi.org/10.1039/d5ra04238k**.

Acknowledgements

H. K. A. Y. would like to thank the Deanship of Graduate Studies and Research, Ajman University, UAE, for their support in providing assistance in article processing charges for this research. The authors gratefully acknowledge the Central Instrumentation Facility (CIF), Savitribai Phule Pune University (SPPU), Pune, for providing instrumental support for FT-IR, ^{1}H NMR, ^{13}C{^{1}H} NMR, ^{19}F NMR, and HRMS analyses. The authors gratefully acknowledge the Research Centre in Chemistry, MGV's Loknete Vyankatrao Hiray Arts, Science and Commerce College, Panchavati, Nashik and Department of Chemistry, Dr Patangrao Kadam Mahavidyalaya, Ramanandanagar (Burli), Palus for providing research facilities and infrastructure. The authors also thank Department of Microbiology, Sant Gadge Baba Amravati University for microbiological studies. D.Y. Patil University, Navi Mumbai, and Chettinad Academy of Research and Education is also acknowledged for their valuable support. The authors sincerely thank the Maratha Mandal's Central Research Laboratory (MMCRL), Belgaum, Karnataka, for providing antitubercular studies.

References

1 T. Qadir, A. Amin, P. K. Sharma, I. Jeelani and H. Abe, A review on medicinally important heterocyclic compounds, *Open Med. Chem. J.*, 2022, **16**(1), e187410452202280.
2 E. Kabir and M. Uzzaman, A review on biological and medicinal impact of heterocyclic compounds, *Results Chem.*, 2022, **4**, 100606.
3 O. Ebenezer, M. A. Jordaan, G. Carena, T. Bono, M. Shapi and J. A. Tuszynski, An overview of the biological evaluation of selected nitrogen-containing heterocycle medicinal chemistry compounds, *Int. J. Mol. Sci.*, 2022, **23**(15), 8117.
4 A. F. Kassem, R. H. Althomali, M. M. Anwar and W. I. El-Sofany, Thiazole moiety: A promising scaffold for anticancer drug discovery, *J. Mol. Struct.*, 2024, **1303**, 137510.
5 R. Raveesha, A. M. Anusuya, A. V. Raghu, K. Y. Kumar, M. D. Kumar, S. B. Prasad and M. K. Prashanth, Synthesis and characterization of novel thiazole derivatives as potential anticancer agents: Molecular docking and DFT studies, *Comput. Toxicol.*, 2022, **21**, 100202.
6 N. Bhanwala, V. Gupta, L. Chandrakar and G. L. Khatik, Thiazole heterocycle: an incredible and potential scaffold in drug discovery and development of antitubercular agents, *ChemistrySelect*, 2023, **8**(46), e202302803.
7 K. Veena, M. S. Raghu, K. Y. Kumar, C. P. Kumar, F. A. Alharti, M. K. Prashanth and B. H. Jeon, Design and synthesis of novel benzimidazole linked thiazole derivatives as promising inhibitors of drug-resistant tuberculosis, *J. Mol. Struct.*, 2022, **1269**, 133822.
8 R. E. Khidre and I. A. M. Radini, Design, synthesis and docking studies of novel thiazole derivatives incorporating pyridine moiety and assessment as antimicrobial agents, *Sci. Rep.*, 2021, **11**(1), 7846.
9 K. B. Gangurde, R. A. More, V. A. Adole, R. Rajesh, S. N. Mali, S. S. Gurav and D. S. Ghotekar, Thiazole derivatives as promising antimicrobial and antioxidant agents: insights from synthesis, bioactivity, and computational studies, *J. Sulfur Chem.*, 2025, **46**(4), 673–698.
10 M. M. Al-Sanea, M. S. Abdel-Maksoud, M. F. El-Behairy, A. Hamdi, H. U. Rahman, D. G. Parambi, R. M. Elbargisy and A. A. Mohamed, Anti-inflammatory effect of 3-fluorophenyl pyrimidinylimidazo[2,1-b]thiazole derivatives as p38α inhibitors, *Bioorg. Chem.*, 2023, **139**, 106716.
11 F. Lemilemu, M. Bitew, T. B. Demissie, R. Eswaramoorthy and M. Endale, Synthesis, antibacterial and antioxidant

activities of thiazole-based Schiff base derivatives: a combined experimental and computational study, *BMC Chem.*, 2021, **15**(1), 67.

12 K. Singh, R. Pal, S. A. Khan, B. Kumar and M. J. Akhtar, Insights into the structure activity relationship of nitrogen-containing heterocyclics for the development of antidepressant compounds: an updated review, *J. Mol. Struct.*, 2021, **1237**, 130369.

13 V. Kovalishyn, O. Severin, M. Kachaeva, I. Semenyuta, K. A. Keith, E. A. Harden, *et al.*, Design and experimental validation of the oxazole and thiazole derivatives as potential antivirals against human cytomegalovirus, *SAR QSAR Environ. Res.*, 2023, **34**(7), 523–541.

14 M. A. Abid, A. A. Abed, M. Musa, T. Izuagie and E. C. Agwamba, Anti-diabetic, anti-bacterial and anti-oxidant potential of new biologically active thiazole-derivatives: experimental and molecular docking studies, *J. Mol. Struct.*, 2025, **1321**, 139482.

15 N. D. F. N. Santos, N. D. S. B. Junior, J. F. de Oliveira, D. M. F. A. Duarte, J. C. dos Santos Soares, D. S. C. Marques, *et al.*, Synthesis, characterization, antioxidant and antiparasitic activities of new naphthyl-thiazole derivatives, *Exp. Parasitol.*, 2023, **248**, 108498.

16 E. M. Komyha, W. H. Mahmoud, W. M. Hosny and A. A. El-Sherif, Design, structural characterization, molecular docking and biomedical applications of hydrazone-based Schiff base metal complexes, *Egypt. J. Chem.*, 2023, **66**(13), 1219–1230.

17 A. M. El-Naggar, A. Zidan, E. B. Elkaeed, M. S. Taghour and W. A. Badawi, Design, synthesis and docking studies of new hydrazinyl-thiazole derivatives as anticancer and antimicrobial agents, *J. Saudi Chem. Soc.*, 2022, **26**(4), 101488.

18 A. E. Evren, L. Yurttaş, B. Ekselli, O. Aksoy and G. Akalin-Çiftçi, Design and efficient synthesis of novel 4,5-dimethylthiazole-hydrazone derivatives and their anticancer activity, *Lett. Drug Des. Discovery*, 2021, **18**(4), 372–386.

19 V. Zazharskyi, O. Bigdan, V. Parchenko, M. Parchenko, T. Fotina, P. Davydenko, *et al.*, Antimicrobial activity of some furans containing 1,2,4-triazoles, *J. Res. Pharm. Pract.*, 2021, **12**(2), 60–65.

20 D. Osmaniye, Ş. Karaca, B. Kurban, M. Baysal, I. Ahmad, H. Patel, *et al.*, Design, synthesis, molecular docking and molecular dynamics studies of novel triazolothiadiazine derivatives containing furan or thiophene rings as anticancer agents, *Bioorg. Chem.*, 2022, **122**, 105709.

21 Y. Sicak, Design and antiproliferative and antioxidant activities of furan-based thiosemicarbazides and 1,2,4-triazoles: their structure-activity relationship and SwissADME predictions, *Med. Chem. Res.*, 2021, **30**(8), 1557–1568.

22 H. M. Pallavi, F. H. Al-Ostoot, H. K. Vivek and S. A. Khanum, Synthesis, characterization, DFT, docking studies and molecular dynamics of some 3-phenyl-5-furan isoxazole derivatives as anti-inflammatory and anti-ulcer agents, *J. Mol. Struct.*, 2022, **1250**, 131812.

23 H. N. Akolkar, S. G. Dengale, K. K. Deshmukh, B. K. Karale, N. R. Darekar, V. M. Khedkar and M. H. Shaikh, Design, synthesis and biological evaluation of novel furan & thiophene containing pyrazolyl pyrazolines as antimalarial agents, *Polycyclic Aromat. Compd.*, 2022, **42**(5), 1959–1971.

24 M. T. Helmy, F. M. Sroor, A. M. Othman, H. M. Hassaneen, F. M. Saleh and M. A. M. Teleb, Design, synthesis and in-vitro evaluation of new furan-substituted thiadiazolyl hydrazone derivatives as promising antimicrobial agents, *J. Heterocycl. Chem.*, 2023, **60**(4), 585–595.

25 V. V. H. Le and J. Rakonjac, Nitrofurans: Revival of an "old" drug class in the fight against antibiotic resistance, *PLoS Pathog.*, 2021, **17**(7), e1009663.

26 S. Cascioferro, B. Parrino, D. Carbone, D. Schillaci, E. Giovannetti, G. Cirrincione and P. Diana, Thiazoles, their benzofused systems, and thiazolidinone derivatives: versatile and promising tools to combat antibiotic resistance, *J. Med. Chem.*, 2020, **63**(15), 7923–7956.

27 S. Rezaei, S. Akbari, F. Rahmani, S. Varnousfaderani, S. Gomroki and E. Jafarzadeh, Nitrofurans as potent antibacterial agents: a systematic review of literature, *Int. J. Adv. Biol. Biomed. Res.*, 2022, **10**, 126–138.

28 A. Kashyap, N. Adhikari, A. Das, A. Shakya, S. K. Ghosh, U. P. Singh and H. R. Bhat, Review on synthetic chemistry and antibacterial importance of thiazole derivatives, *Curr. Drug Discovery Technol.*, 2018, **15**(3), 214–228.

29 G. G. Parra, L. P. Ferreira, D. C. Codognato, C. C. Cavalheiro and I. Borissevitch, Characteristics of the excited states of nitrofurantoin, an anti-inflammatory and photoactive nitrofuran derivative, *J. Lumin.*, 2017, **185**, 10–16.

30 A. Bhatnagar and G. Pemawat, An overview on synthetic routes of anti-inflammatory active scaffolds including thiazole and thiazolidine cores, *Phosphorus, Sulfur Silicon Relat. Elem.*, 2023, **198**(7), 554–565.

31 A. F. Kassem, R. H. Althomali, M. M. Anwar and W. I. El-Sofany, Thiazole moiety: A promising scaffold for anticancer drug discovery, *J. Mol. Struct.*, 2024, **1303**, 137510.

32 J. R. A. D. Queiroz Júnior, J. P. D. Costa Pereira, L. L. Pires and C. S. Maia, The dichotomous effect of thiamine supplementation on tumorigenesis: a systematic review, *Nutr. Cancer*, 2022, **74**(6), 1942–1957.

33 L. V. Vigneswaran, Multidrug resistance complexity of Mycobacterium tuberculosis and oxidative stress: the need for innovative drug delivery strategies, in *Emerging Paradigms in Delivery Systems for Antitubercular Therapy*, Academic Press, 2025, pp. 235–265.

34 B. H. Gulumbe, A. Abdulrahim, S. K. Ahmad, K. A. Lawan and M. B. Danlami, WHO report signals tuberculosis resurgence: addressing systemic failures and revamping control strategies, *Decoding Infect. Transm.*, 2025, **3**, 100044.

35 B. H. Gulumbe, A. Abdulrahim and M. B. Danlami, The United Nations' ambitious roadmap against tuberculosis: opportunities, challenges and the imperative of equity, *Future Sci. OA*, 2024, **10**(1), 2418787.

36 A. Chakraborty, and J. Jayawickrama, History of tuberculosis and contemporary challenges, in *A Brief Social History of Tuberculosis*, Routledge, 2024, pp. 10–24.

37 D. C. Nwobodo, M. C. Ugwu, C. O. Anie, M. T. Al-Ouqaili, C. J. Ikem, V. C. Umeh and M. Saki, Antibiotic resistance: the challenges and some emerging strategies for tackling a global menace, *J. Clin. Lab. Anal.*, 2022, **36**(9), e24655.

38 M. A. Salam, M. Y. Al-Amin, M. T. Salam, J. S. Pawar, N. Akhter, A. A. Rabaan and M. A. Alqumber, Antimicrobial resistance: a growing serious threat for global public health, *Healthcare*, 2023, **11**(13), 1946.

39 H. Fongang, A. T. Mbaveng, and V. Kuete, Global burden of bacterial infections and drug resistance, in *Advances in Botanical Research*, Academic Press, 2023, vol. 106, pp. 1–20.

40 S. K. Ahmed, S. Hussein, K. Qurbani, R. H. Ibrahim, A. Fareeq, K. A. Mahmood and M. G. Mohamed, Antimicrobial resistance: impacts, challenges, and future prospects, *J. Med. Surg. Public Health*, 2024, **2**, 100081.

41 P. P. Kalelkar, M. Riddick and A. J. García, Biomaterial-based antimicrobial therapies for the treatment of bacterial infections, *Nat. Rev. Mater.*, 2022, **7**(1), 39–54.

42 S. Kokanov, M. Nikolić, I. Novaković, T. Todorović and N. Filipović, Synthesis, characterization, and evaluation of antioxidant and antimicrobial activity of three novel N-heteroaromatic hydrazonyl-thiazoles, *Adv. Technol.*, 2021, **10**(2), 14–23.

43 R. A. Shinde, V. A. Adole, G. S. Bagdane, B. S. Jagdale, A. A. R. Mahmood, I. Ahmad, *et al.*, Comprehensive exploration of thiophene-tagged 2-(2-hydrazinyl)thiazole derivatives: synthesis, structural characterization, antimicrobial potential, and computational insights, *J. Mol. Struct.*, 2025, **1341**, 142453.

44 X. Zhang and J. Li, Exploration of the role of computational chemistry in modern drug discovery, *Comput. Mol. Biol.*, 2024, **14**(3), 115–124.

45 G. Anand, M. Sivasubramanian, I. Manimehan, A. Ruby, R. Abinayashri and R. K. Asmitha, Synthesis, spectroscopic elucidation (FT-IR, FT-Raman, UV-vis), quantum chemical computation (PES, FMO, HOMO–LUMO, MEP, NLO, Hirshfeld) and molecular docking studies on 2-thiophenecarboxamide crystal, *J. Mol. Struct.*, 2023, **1286**, 135586.

46 M. Buvaneswari, R. Santhakumari, C. Usha, R. Jayasree and S. Sagadevan, Synthesis, growth, structural, spectroscopic, optical, thermal, DFT, HOMO–LUMO, MEP, NBO analysis and thermodynamic properties of vanillin isonicotinic hydrazide single crystal, *J. Mol. Struct.*, 2021, **1243**, 130856.

47 A. Saral, P. Sudha, S. Muthu, S. Sevvanthi and A. Irfan, Molecular structure spectroscopic elucidation, IEFPCM solvation (UV-Vis, MEP, FMO, NBO, NLO), molecular docking and biological assessment studies of lepidine (4-methylquinoline), *J. Mol. Liq.*, 2022, **345**, 118249.

48 M. Vennila, R. Rathikha, S. Muthu, A. Jeelani and A. Irfan, Theoretical structural analysis (FT-IR, FT-R), solvent effect on electronic parameters NLO, FMO, NBO, MEP, UV (IEFPCM model), Fukui function evaluation with pharmacological analysis on methyl nicotinate, *Comput. Theor. Chem.*, 2022, **1217**, 113890.

49 S. Khan, H. Ullah, M. Taha, F. Rahim, M. Sarfraz, R. Iqbal, *et al.*, Synthesis, DFT studies, molecular docking and biological activity evaluation of thiazole-sulfonamide derivatives as potent Alzheimer's inhibitors, *Molecules*, 2023, **28**(2), 559.

50 S. Saikia and M. Bordoloi, Molecular docking: challenges, advances and its use in drug discovery perspective, *Curr. Drug Targets*, 2019, **20**(5), 501–521.

51 H. G. El-kasabi, M. M. Girges, A. F. El-Sayed and G. E. Abdel-Ghani, Synthesis, anticancer activity, molecular docking, ADMET analysis and dynamic simulations of a novel series of thiazole derivatives based on furan-2-carbaldehyde thiosemicarbazone, *J. Mol. Struct.*, 2025, **1322**, 140004.

52 R. Sghyar, S. M. Basavarajaiah, A. Chda, O. Moussaoui, E. M. El Hadrami, A. Ben-Tama, *et al.*, Design, synthesis, biological evaluation on immune cell proliferation, crystal structures, spectroscopic characterizations, DFT calculations, ADME analysis, and molecular docking studies with COX of novel tetrazole-Galactopyranosyl analogues, *J. Mol. Struct.*, 2023, **1287**, 135695.

53 U. Acar Çevik, I. Celik, A. Işık, I. Ahmad, H. Patel, Y. Özkay, *et al.*, Design, synthesis, molecular modeling, DFT, ADME and biological evaluation studies of some new 1,3,4-oxadiazole linked benzimidazoles as anticancer agents and aromatase inhibitors, *J. Biomol. Struct. Dyn.*, 2023, **41**(5), 1944–1958.

54 L. Golea, R. Chebaki, M. Laabassi and P. Mosset, Synthesis, characterization of some substituted quinolines derivatives: DFT, computational, *in silico* ADME, molecular docking and biological activities, *Chem. Data Collect.*, 2023, **43**, 100977.

55 M. C. Lourenco, M. V. de Souza, A. C. Pinheiro, M. D. L. Ferreira, R. S. Gonçalves, T. C. M. Nogueira, *et al.*, Evaluation of anti-tubercular activity of nicotinic and isoniazid analogues, *Arkivoc*, 2007, **15**, 181–191.

56 A. W. Bauer, W. M. M. Kirby, J. C. Sherris and M. Turck, Antibiotic susceptibility testing by a standardized single disk method, *Am. J. Clin. Pathol.*, 1966, **45**(4_ts), 493–496.

57 P. Wayne, Clinical and Laboratory Standards Institute (CLSI) (2020) Performance standards for antimicrobial susceptibility testing: Background, organization, functions, and processes, *J. Clin. Microbiol.*, 2010, **58**(3), 01864–0186419.

58 L. M. Podust, T. L. Poulos and M. R. Waterman, Crystal structure of cytochrome P450 14alpha-sterol demethylase (CYP51) from Mycobacterium tuberculosis in complex with azole inhibitors, *Proc. Natl. Acad. Sci. U. S. A.*, 2001, **98**(6), 3068–3073.

59 M. Chalkha, H. Nour, K. Chebbac, A. Nakkabi, L. Bahsis, M. Bakhouch, *et al.*, Synthesis, characterization, DFT mechanistic study, antimicrobial activity, molecular modeling, and ADMET properties of novel pyrazole-isoxazoline hybrids, *ACS Omega*, 2022, **7**(50), 46731–46744.

60 M. S. Alam and J. U. Ahmed, Synthesis, crystal structure, biological evaluation, *in silico* ADME properties, enzymatic target prediction and molecular docking studies of pyrazolone-azomethine analogs, *J. Mol. Struct.*, 2023, **1294**, 136504.

61 Y. R. Sable, V. A. Adole, E. A. Pithawala and R. D. Amrutkar, Design, synthesis, and antitubercular evaluation of

piperazinyl-pyrazolyl-2-hydrazinyl thiazole derivatives: Experimental, DFT and molecular docking insights, *J. Sulfur Chem.*, 2025, **46**(3), 513–538.

62 M. M. Abdelall, Synthesis of 1,3,4-thiadiazoles, α-pyranone, pyridine, polysubstituted benzene from 1,3,4-thiadiazolyl ethanone and testing against tuberculosis based on molecular docking studies, *Orient. J. Chem.*, 2014, **30**(3), 1099–1109.

63 K. M. Chandrika and P. V, An *in silico* molecular docking, ADMET and molecular dynamics simulations studies of azolyl-2H-chroman-4-ones as potential inhibitors against pathogenic fungi and bacteria, *J. Biomol. Struct. Dyn.*, 2024, **42**(15), 7667–7685.

64 R. Huey, G. M. Morris, and S. Forli, Using AutoDock 4 and AutoDock vina with AutoDockTools: a tutorial, *Scripps Research Institute's Molecular Graphics Laboratory*, 2012;10550(92037):1000.

65 E. D. Boittier, Y. Y. Tang, M. E. Buckley, Z. P. Schuurs, D. J. Richard and N. S. Gandhi, Assessing molecular docking tools to guide targeted drug discovery of CD38 inhibitors, *Int. J. Mol. Sci.*, 2020, **21**, 5183.

66 A. Daina, O. Michielin and V. Zoete, SwissADME: a free web tool to evaluate pharmacokinetics, drug-likeness and medicinal chemistry friendliness of small molecules, *Sci. Rep.*, 2017, **7**(1), 42717.

67 V. A. Adole, A. Kumar, N. Misra, R. A. Shinde and B. S. Jagdale, Synthesis, computational, antimicrobial, antioxidant, and ADME study of 2-(3,4-dimethoxyphenyl)-4H-chromen-4-one, *Polycyclic Aromat. Compd.*, 2023, **44**(8), 5397–5411.

68 K. B. Gangurde, V. A. Adole and D. S. Ghotekar, Computational study: Synthesis, spectroscopic (UV–vis, IR, NMR), antibacterial, antifungal, antioxidant, molecular docking and ADME of new (E)-5-(1-(2-(4-(2,4-dichlorophenyl)thiazol-2-yl)hydrazineylidene)ethyl)-2,4-dimethylthiazole, *Results Chem.*, 2023, **6**, 101093.

69 V. A. Adole, Computational approach for the investigation of structural, electronic, chemical and quantum chemical facets of twelve Biginelli adducts, *Organomet. Chem.*, 2021, **1**(1), 29–40.

70 M. J. Frisch, G. W. Trucks, H. B. Schlegel, G. E. Scuseria, M. A. Robb, J. R. Cheeseman, *et al.*, *Gaussian 03, Revision C.02*, Gaussian Inc., Wallingford CT, 2004.

71 A. D. Becke, Density-functional thermochemistry. III. The role of exact exchange, *J. Chem. Phys.*, 1993, **98**(7), 5648–5652.

72 C. Lee, W. Yang and R. G. Parr, Development of the Colle-Salvetti correlation-energy formula into a functional of the electron density, *Phys. Rev. B:Condens. Matter Mater. Phys.*, 1988, **37**(2), 785.

73 R. D. I. I. Dennington, T. Keith, and J. Millam, *GaussView*, Version 4.1.2, Semichem Inc., Shawnee Mission, KS, 2007.

74 Y. R. Sable, V. A. Adole, R. A. Shinde, H. S. Deshmukh, R. Rajesh, T. M. Almutairi, *et al.*, Exploring pyrazole integrated thiazole molecular hybrids for antitubercular activity: Synthesis, spectral characterization, DFT, ADME, and docking studies, *J. Mol. Struct.*, 2025, **1344**, 142891.

75 R. Matsa, P. Makam, G. Sethi, A. A. Thottasseri, A. R. Kizhakkandiyil, K. Ramadas, *et al.*, Pyridine appended 2-hydrazinylthiazole derivatives: Design, synthesis, *in vitro* and *in silico* antimycobacterial studies, *RSC Adv.*, 2022, **12**(29), 18333–18346.

76 A. M. Hussein, S. M. Gomha, N. A. A. El-Ghany, M. E. Zaki, B. Farag, S. A. Al-Hussain, *et al.*, Green biocatalyst for ultrasound-assisted thiazole derivatives: Synthesis, antibacterial evaluation, and docking analysis, *ACS Omega*, 2024, **9**(12), 13666–13679.

77 L. M. Podust, J. Stojan, T. L. Poulos and M. R. Waterman, Substrate recognition sites in 14α-sterol demethylase from comparative analysis of amino acid sequences and X-ray structure of Mycobacterium tuberculosis CYP51, *J. Inorg. Biochem.*, 2001, **87**(4), 227–235.

78 K. J. McLean, A. J. Dunford, R. Neeli, M. D. Driscoll and A. W. Munro, Structure, function and drug targeting in Mycobacterium tuberculosis cytochrome P450 systems, *Arch. Biochem. Biophys.*, 2007, **464**(2), 228–240.

79 H. S. Deshmukh, V. A. Adole, S. N. Mali and B. S. Jagdale, Design, synthesis, biological evaluation, and computational insights of 2-(Aryl)benzo[d]imidazo[2,1-b]thiazole-7-sulfonamide derivatives as potent antitubercular and antibacterial agents, *BMC Chem.*, 2025, **19**(1), 1–17.

80 V. A. Adole, I. A. Danish, J. J. Kores, J. W. Jebaraj, S. Janani, S. K. Ghotekar, *et al.*, Computational and experimental exploration of morpholine pendent 2-hydrazineyl thiazole: Insights from DFT, ADME profiling, antifungal efficacy and molecular docking analyses, *Results Chem.*, 2025, **13**, 101951.